JEM Journal of Experimental Medicine

ARTICLE

Cbl and Cbl-b control the germinal center reaction by facilitating naive B cell antigen processing

Xin Li[1,2], Liying Gong[1,3], Alexandre P. Meli[4], Danielle Karo-Atar[4], Weili Sun[1,3], Yongrui Zou[5], Irah L. King[4], and Hua Gu[1,2,3]

Antigen uptake and presentation by naive and germinal center (GC) B cells are different, with the former expressing even low-affinity BCRs efficiently capture and present sufficient antigen to T cells, whereas the latter do so more efficiently after acquiring high-affinity BCRs. We show here that antigen uptake and processing by naive but not GC B cells depend on Cbl and Cbl-b (Cbls), which consequently control naive B and cognate T follicular helper (Tfh) cell interaction and initiation of the GC reaction. Cbls mediate CD79A and CD79B ubiquitination, which is required for BCR-mediated antigen endocytosis and postendocytic sorting to lysosomes, respectively. Blockade of CD79A or CD79B ubiquitination or Cbls ligase activity is sufficient to impede BCR-mediated antigen processing and GC development. Thus, Cbls act at the entry checkpoint of the GC reaction by promoting naive B cell antigen presentation. This regulation may facilitate recruitment of naive B cells with a low-affinity BCR into GCs to initiate the process of affinity maturation.

Introduction

High-affinity antibody-producing B cells are generated in germinal centers (GCs), where B cells with low-affinity B cell antigen receptors (BCRs) acquire increased receptor affinity by somatic hypermutation (SHM) of their immunoglobulin variable region genes through selection by antigen-specific T cells and clonal expansion (Allen et al., 2007; Jacob et al., 1991; Liu et al., 1989; Rajewsky, 1996; Victora and Nussenzweig, 2012). Ample evidence indicates that the ability of B cells to uptake antigen via the BCR and present antigen to T cells is critical for determining different cellular responses (Crotty, 2011; Shulman et al., 2014). At the entry of the GC reaction, antigen-specific naive B cells capture antigen from macrophages or dendritic cells (DCs) and present the antigen to $CD4^+$ T cells activated by DCs (Crotty, 2011; Shulman et al., 2014; Watanabe et al., 2017). B cells capturing sufficient antigen at this stage establish proper T–B cell interaction, which elicits the proliferate of cognate B and T cells and further development into GC B and T follicular helper (Tfh) cells, respectively. Within GCs, developing GC B cells acquire different quantities of antigen from follicular DCs (FDCs) based on their BCR affinity for the antigen and present it to Tfh cells. This interaction stimulates B cell SHM that may result in an increase in BCR affinity, leading to additional help from Tfh cells. These molecular events result in GC B cell expansion and eventually differentiation into antibody-secreting plasma cells (PCs) or memory B cells (Gitlin et al., 2014; Meyer-Hermann et al., 2012; Rajewsky, 1996; Schwickert et al., 2007; Victora and Nussenzweig, 2012). The cognate T–B cell interactions within the GC also involve several pairs of costimulatory receptors and ligands, such as inducible T cell costimulator (ICOS)–ICOS ligand (ICOSL), CD40–CD40L, and LFA-1–ICAM1 (Choi et al., 2011; De Silva and Klein, 2015; Meli et al., 2016; Shlomchik and Weisel, 2012a; Victora and Nussenzweig, 2012; Zotos and Tarlinton, 2012). However, the ability of B cells to capture, process, and present sufficient antigen in the form of MHC–peptide complexes to T cells appears to play a central role in determining B cell fate at different stages of the GC reaction.

Unlike professional APCs, which acquire antigen nonspecifically, B cells capture and process antigens mainly through the BCR (Batista and Harwood, 2009; Lanzavecchia, 1990; Phan et al., 2007). Stimulation of the BCR by antigens has two consequences. First, in concert with appropriate costimulation, it activates the BCR signaling cascade, leading to gene transcription required for cell proliferation and differentiation (Khalil et al., 2012; Kräutler et al., 2017; Kurosaki et al., 2010; Shlomchik and Weisel, 2012a; Victora and Nussenzweig, 2012). Second, it enables antigen uptake and processing through BCR-mediated antigen endocytosis and postendocytic sorting into lysosomes for degradation (Batista and Harwood, 2009; Lankar

[1]Montreal Clinical Research Institute, Montreal, Quebec, Canada; [2]Department of Microbiology and Immunology, Department of Biochemistry and Molecular Medicine, University of Montreal, Montreal, Quebec, Canada; [3]Division of Experimental Medicine, McGill University, Montreal, Quebec, Canada; [4]Department of Microbiology and Immunology, Meakins-Christie Laboratories, McGill University Health Center, Montreal, Quebec, Canada; [5]The Feinstein Institute for Medical Research, Manhasset, New York, NY.

Correspondence to H. Gu: hua.gu@ircm.qc.ca.

et al., 2002; Stoddart et al., 2002; Victora and Nussenzweig, 2012; Yuseff et al., 2013). Recent studies have shown a striking functional difference between naive and GC B cells with respect to BCR-mediated antigen uptake and processing. Naive B cells expressing either high- or low-affinity BCRs effectively internalize antigens (Kwak et al., 2018). This property allows even those B cells expressing low-affinity BCRs to capture and present sufficient antigen for productive engagements with cognate T cells. In contrast, the affinity threshold for BCR internalization in GC B cells is much higher relative to naive B cells. As a result, GC B cells with high-affinity BCRs are much more competent to capture and present sufficient antigen to Tfh cells (Kwak et al., 2018; Nowosad et al., 2016). A fundamental question raised by these observations is whether BCR-mediated antigen processing is controlled by distinct intracellular regulatory signals in naive and GC B cells. The BCR (IgM) contains a very short cytoplasmic tail and must constitutively associate with transmembrane signaling modules CD79A and CD79B. While it is well established that BCR signaling depends on both CD79A and CD79B, little is known about the regulation that controls BCR-mediated antigen-endocytic and postendocytic trafficking. While recent studies have shown that both CD79A and CD79B can be ubiquitinated (Kitaura et al., 2007; Zhang et al., 2007), the mechanisms and biological consequences of this posttranslational modulation have yet to be elucidated.

Cbl and Cbl-b (Cbls) belong to the superfamily of E3 ubiquitin ligases and exert their regulatory roles through both ubiquitin ligase and scaffolding functions (Huang and Gu, 2008). In B cells, Cbls control antibody affinity maturation by regulating the exit checkpoint of the GC reaction in GC B cells (Li et al., 2018). Here, we show that B cell–intrinsic Cbls are essential regulators of the GC entry checkpoint. We find that Cbls facilitate naive B cell antigen presentation and are essential for the cognate interaction between naive B and T cells. In the absence of Cbls, BCR-mediated endocytic and postendocytic antigen trafficking to lysosomes are blocked, rendering B cells incapable of interacting with T cells and developing into GC B cells. We further identify that Cbls regulate these processes by promoting ubiquitination of CD79A and CD79B, which are respectively responsible for the endocytic and postendocytic transport of BCR–antigen complexes to late endosome/lysosomes. Notably, these regulatory processes are operational in naive, but not GC, B cells, thus suggesting an explanation for the long-standing enigma regarding the distinct dynamics of antigen uptake in differentiating B cell subsets.

Results

Ablation of Cbls in naive B cells impairs T cell–dependent antibody responses and the GC reaction

Our biochemical studies showed that both Cbls are expressed at different stages of peripheral B cells (Fig. S1 A). To examine the function of Cbls in the initiation of antibody responses, we generated *Cbl*$^{flox/flox}$ *Cbl-b*$^{-/-}$ *Mb1-Cre* transgenic (Tg; termed Cbl$^{-/-}$Cbl-b$^{-/-}$) mice in which Cbls double mutations occurred only in B cells (Fig. S1 B). Inspection of the B cell compartment in Cbl$^{-/-}$Cbl-b$^{-/-}$ mice revealed that the development of follicular B cells was normal. By contrast, the number of marginal zone (MZ) B cells was severely reduced and that of bone marrow B cells and B1b cells were slightly increased compared with controls (Fig. S1, C–E). To examine whether the Cbl$^{-/-}$Cbl-b$^{-/-}$ mutation affected humoral immune responses, we immunized WT (*Mb1-Cre Tg*) and Cbl$^{-/-}$Cbl-b$^{-/-}$ mice with T cell–independent or T cell–dependent antigens. Consistent with the lack of MZ B cells, Cbl$^{-/-}$Cbl-b$^{-/-}$ mice failed to mount type-II T cell–independent anti-NP responses after immunization with (4-hydroxy-3-nitrophenyl) acetyl (NP) Ficoll (Fig. S1 F). Additionally, despite having normal numbers of follicular B cells, Cbl$^{-/-}$Cbl-b$^{-/-}$ mutant mice produced significantly less total and high-affinity anti-NP IgG1 antibodies after immunization with the T cell–dependent antigen NP-KLH relative to WT controls (Fig. 1 A). To examine whether defective T cell–dependent antibody production was caused by an impairment in GC development, we examined GC B cell numbers at various time points after immunization by flow cytometry. We found that Cbl$^{-/-}$Cbl-b$^{-/-}$ mice developed a significantly reduced number of GC B cells (B220^{+}IgD^{-}GL7^{+}FAS^{hi}) at day 4 relative to WT controls and failed to expand the GC B cell population as vigorously as WT mice thereafter (Fig. 1, B and C). Consequently, numbers of antibody-secreting PCs producing total (anti-NP$_{30}$) or high affinity (anti-NP$_{4}$) IgG1 antibodies in the spleen of the mutant mice were also reduced relative to that in WT mice (Fig. 1 D). A similar deficiency in GC B cell numbers was found when mice were immunized with a high dose of T cell–dependent antigen, sheep RBCs (SRBCs; Fig. 1 E). This suggests that the deficiency is unlikely caused by an insufficient amount of antigen. Together, our results indicate that Cbl proteins control the initial entry and expansion of B cells in GCs. Since GC B cell development was normal in Cbl$^{-/-}$ or Cbl-b$^{-/-}$ mice (Fig. 1 E), we conclude that this function is shared by Cbls.

The Cbl$^{-/-}$Cbl-b$^{-/-}$ mutation impairs the development of Tfh cells and cognate T–B cell interactions

Development of GCs depends on the overall architecture of lymphoid follicles and clonal expansion of B cells driven by BCR signaling (Jang et al., 2011; Shlomchik and Weisel, 2012b; Victora and Nussenzweig, 2012). In addition, it also requires help from cognate Tfh cells that produce CD40L, IL-4 and IL-21 after Tfh cell activation (Crotty, 2011; Shulman et al., 2014). To understand the cause of defective GC development in Cbl$^{-/-}$Cbl-b$^{-/-}$ mice, we examined whether the Cbl$^{-/-}$Cbl-b$^{-/-}$ mutation impacted these events in both ex vivo and in vivo assays. We found that Cbl$^{-/-}$Cbl-b$^{-/-}$ mice exhibited a normal distribution of T, B, and CD35^{+} FDCs but reduced MZ macrophages in the spleen as compared with WT controls (Fig. S1, D, E, and G; and Fig. S2 A). In addition, mutant B cells proliferated as efficiently as WT counterparts upon anti-IgM or CD40L stimulation (Fig. S2 B and C). In contrast, we found that the Cbl$^{-/-}$Cbl-b$^{-/-}$ mutation impaired Tfh cell development, as the mutant mice had significantly lower numbers of TCR-β^{+}CD4^{+}CXCR5^{hi}PD1^{hi} Tfh cells compared with WT controls (Fig. 2 A). This alteration was not likely caused by the germline mutation of Cbl-b, because Cbl-b$^{-/-}$ mice possessed normal numbers of Tfh cells (Fig. 2 A). Tfh cells from Cbl$^{-/-}$Cbl-b$^{-/-}$ mice also expressed a lower amount of BCL6 relative to WT Tfh cells (Fig. 2 B), consistent with a failure to generate mature Tfh cells. To

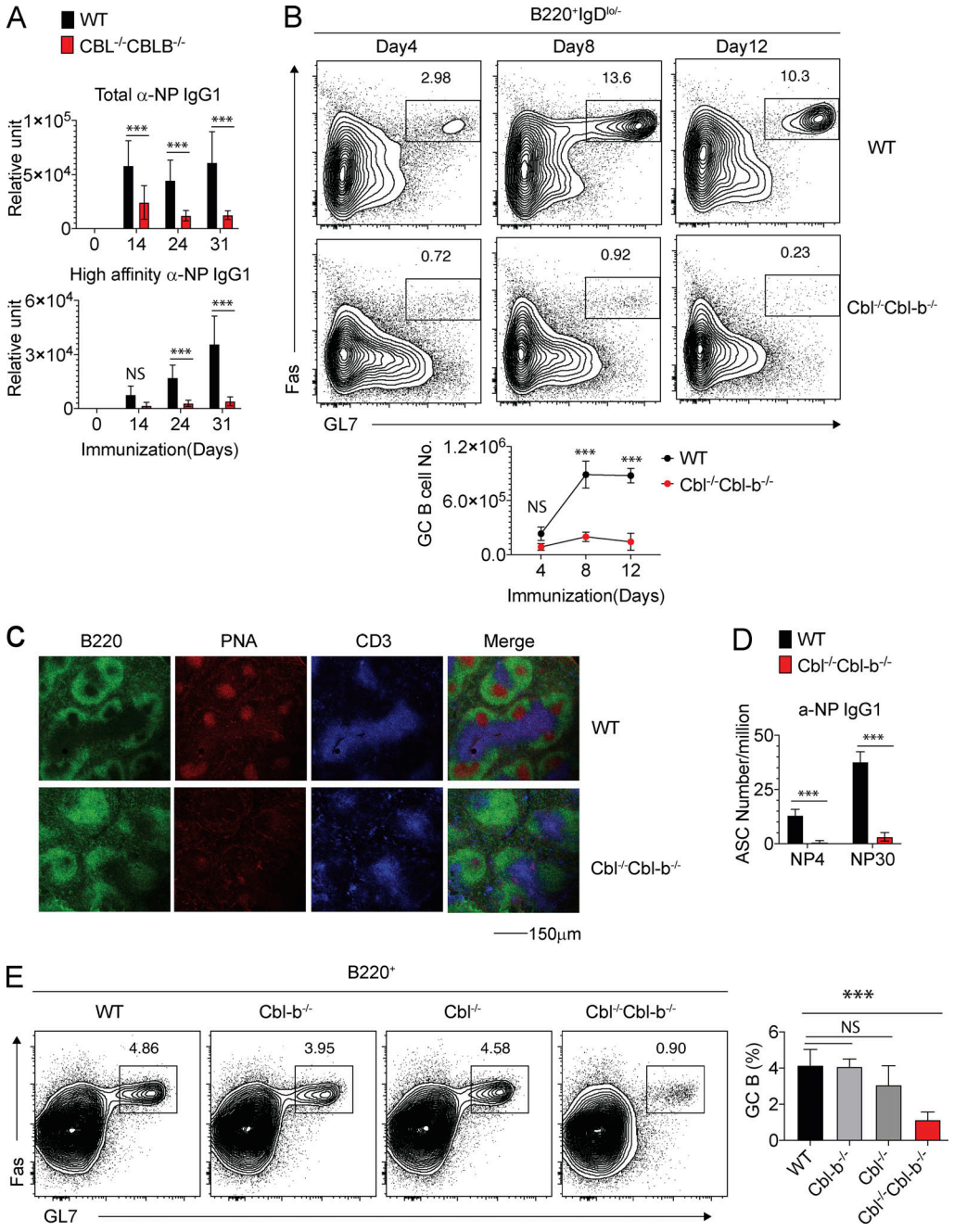

Figure 1. **Impaired T cell–dependent antibody responses and GC development in Cbl$^{-/-}$Cbl-b$^{-/-}$ mice. (A)** The kinetics of total and high-affinity anti-NP responses of the IgG1 isotype in WT (*Mb1-Cre* Tg) and Cbl$^{-/-}$Cbl-b$^{-/-}$ mice after NP-KLH immunization. Shown are ELISA results of serum titers of the total (anti-NP$_{30}$) and high-affinity (anti-NP$_4$) IgG1 antibodies (n = 6). **(B)** Flow cytometric analyses of splenic GC B cell development in WT (*Mb1-Cre* Tg) and Cbl$^{-/-}$Cbl-b$^{-/-}$ mice after NP-KLH immunization. Shown are contour maps (top) and kinetics (bottom) of Fas$^+$GL7^{hi} GC B cells in the gated B220$^+$IgD$^-$ B cells (n = 5). **(C)** Immunofluorescent staining of GCs in the spleen of WT (*Mb1-Cre* tg) and Cbl$^{-/-}$Cbl-b$^{-/-}$ mice at day 10 after NP-KLH immunization. Spleen sections were stained with peanut agglutinin (PNA; red), anti-CD3ε (blue), and anti-B220 (green). Shown are representative images of more than three independent experiments (n = 5). **(D)** Total numbers of splenic antibody-secreting cells (ASCs) against the total NP (NP$_{30}$) or high-affinity NP (NP$_4$) antigen (n = 5). **(E)** Flow cytometric analyses of splenic GC B cells in WT (C57BL/6), Cbl$^{-/-}$, Cbl-b$^{-/-}$, and Cbl$^{-/-}$Cbl-b$^{-/-}$ mice at day 10 after SRBC immunization. Shown are FACS contour maps (left) and statistics (right) of Fas$^+$GL7^{hi} GC B cells in gated B220$^+$IgD$^-$ B cells (n = 5). Data are shown as means ± SD (A, B, D, and E) and from two independent experiments (A, D, and E) and three independent experiments (B and C). ***, P < 0.001 (A and D, unpaired Student's t test; B, two-way ANOVA multiple comparison test; E, one-way ANOVA multiple comparison test).

further characterize the Tfh cell compartment, we examined OT-II TCR Tg T cells carrying both the IL21^{Kat} and IL4^{GFP} reporters that allow for simultaneous detection of different developmental stages of Tfh cells based on IL21^{Kat} and IL4^{GFP} expression (Fig. S2 D; Weinstein et al., 2016). We transferred purified OT-II TCR Tg IL21^{Kat} IL4^{GFP} CD4$^+$ T cells into WT and Cbl$^{-/-}$Cbl-b$^{-/-}$ mice, immunized the recipients with NP-OVA, and then examined GFP$^+$ and/or Kat$^+$ Tfh cells by flow cytometry and confocal microscopy. We found that

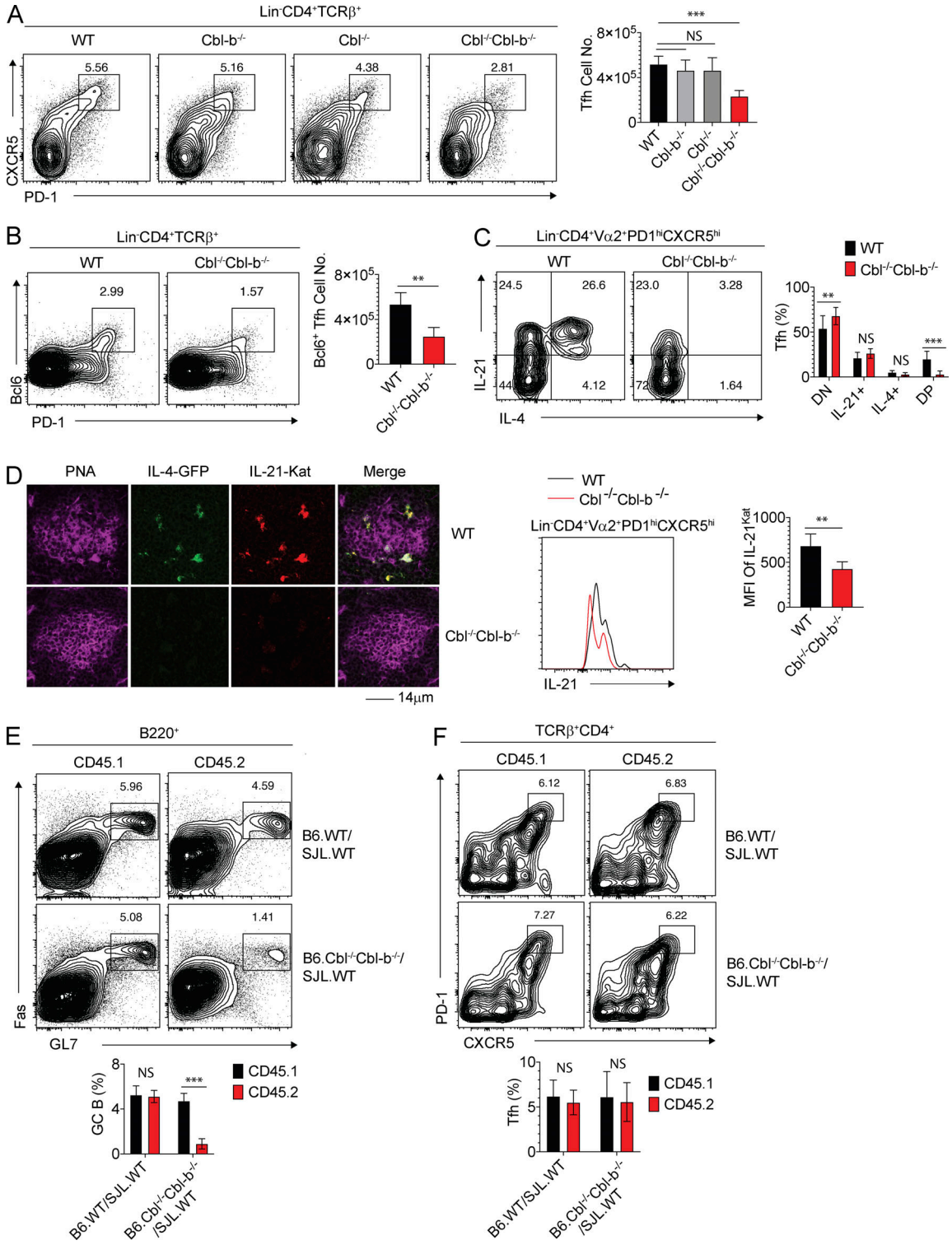

Figure 2. **Incapability of Cbl$^{-/-}$Cbl-b$^{-/-}$ B cells in promoting Tfh cell maturation and receiving help from Tfh cells. (A)** Flow cytometric analyses of splenic Tfh cells in SRBC immunized mice. Shown are FACS analysis (top) and statistics (bottom) of PD-1 vs. CXCR5 staining of splenic (PD-1^{hi}CXCR5^{hi}) Tfh cells among the gated CD4$^+$ T cells (n = 5). **(B)** Expression of Bcl6 in Tfh cells from Cbl$^{-/-}$Cbl-b$^{-/-}$ mice. Shown are a FACS analyses of CXCR5 vs. Bcl6 staining of Tfh cells in gated splenic CD4$^+$ T cells from WT and Cbl$^{-/-}$Cbl-b$^{-/-}$ mice after NP-KLH immunization (n = 5). **(C)** Impaired Tfh cell maturation in WT and Cbl$^{-/-}$Cbl-b$^{-/-}$ OT-II IL21^{Kat} IL4^{GFP} reporter chimeric mice. IL21^{Kat}IL4^{GFP} OT-II CD4$^+$ reporter T cells were transferred into WT and Cbl$^{-/-}$Cbl-b$^{-/-}$ recipient mice, respectively, immunized, and analyzed by FACS. Shown are FACS contour map (top left) and statistics (top right) of OT-II IL21^{Kat+} and IL4^{GFP+} Tfh cells and histogram comparison of IL21^{Kat+} Tfh cells (bottom) in WT and Cbl$^{-/-}$Cbl-b$^{-/-}$ mice after NP-OVA immunization (n = 6). DN, IL-21$^-$IL-4$^-$double negative; DP, IL-21$^+$IL-4$^+$ double positive. **(D)** Immunofluorescent staining of IL21^{Kat}IL4^{GFP} T cells in GCs of the immunized WT and Cbl$^{-/-}$Cbl-b$^{-/-}$ mice (n = 3). **(E and F)** Flow cytometric analyses of GC B and Tfh cells in WT B6:SJL and Cbl$^{-/-}$Cbl-b$^{-/-}$:SJL BM chimeras. Shown are FACS contour maps (top) and statistics (bottom) of GC B cells (E) and Tfh cells (F) derived from SJL, WT B6, and Cbl$^{-/-}$Cbl-b$^{-/-}$ donors, respectively (n = 5). Data are means ± SD (A–C, E, and F) and are

from at two independent experiments (A–D) and three independent experiments (E and F). **, P < 0.01; ***, P < 0.001 (B, C, E, and F, unpaired Student's *t* test; A, one-way ANOVA multiple comparison test).

while the reporter T cells efficiently developed into both IL21$^+$IL4$^-$ immature and IL21$^+$IL4$^+$ mature Tfh cells in WT recipients, the same reporters gave rise to only IL21$^+$ immature Tfh cells that also expressed significantly lower levels of IL21^{Kat} in Cbl$^{-/-}$Cbl-b$^{-/-}$ mice relative to WT controls (Fig. 2, C and D; and Fig. S2 E).

The lack of mature Tfh cells in Cbl$^{-/-}$Cbl-b$^{-/-}$ mice prompted us to ask whether the impaired Tfh cell development was responsible for the defective GC development. To address this question, we examined whether presence of normal Tfh cells could rescue the development of Cbl$^{-/-}$Cbl-b$^{-/-}$ B cells into GC B cells. To this end, we generated bone marrow (BM) chimeric mice reconstituted with an equal number of WT B6.SJL (CD45.1$^+$) and C57BL Cbl$^{-/-}$Cbl-b$^{-/-}$ (CD45.2$^+$) BM hematopoietic stem cells so that the resulting mice contained both WT and Cbl$^{-/-}$Cbl-b$^{-/-}$ B cells in addition to WT T cells. We then immunized the BM chimeras and analyzed GC B and Tfh cells derived from different donors by flow cytometry (Fig. 2, E and F). We found that the immunization induced similar numbers of CD45.1$^+$ and CD45.2$^+$ Tfh cells in the BM chimera, indicating that WT (CD45.1$^+$) B cells in the BM chimeras support the development of both CD45.1$^+$ and CD45.2$^+$ Tfh cells. However, despite the presence of normal Tfh cells and normal numbers of WT (CD45.1$^+$) GC B cells, the numbers of Cbl$^{-/-}$Cbl-b$^{-/-}$ (CD45.2$^+$) GC B cells were reduced, indicating that the mutant B cells are intrinsically deficient in receiving help from Tfh cells. Taken together, we conclude that the Cbl$^{-/-}$Cbl-b$^{-/-}$ mutation does not significantly alter the spleen architecture or B cell proliferation induced by BCR and CD40 signaling. Instead, it impairs the ability of B cells to support the development of, as well as receive help from, cognate Tfh cells.

Cbls control antigen presentation by naive, but not activated, B cells to T cells

Cognate T–B cell interactions in the GC reaction involve initial engagement of the TCR and costimulatory receptors such as ICOS on cognate T cells by MHC-II-peptide antigen and ICOSL expressed on B cells, respectively (Choi et al., 2011). These stimuli up-regulate CD40L on Tfh cells, which in turn stimulates CD40 expressed by B cells and drives GC B cell proliferation (Gitlin et al., 2014). Since we identified that Cbl$^{-/-}$Cbl-b$^{-/-}$ B cells expressed normal amounts of MHC-II, ICOSL, CD40, and CD86 (Fig. S3 A), we decided to examine whether Cbl$^{-/-}$Cbl-b$^{-/-}$ B cells were able to process and present antigen to cognate T cells. For this purpose, we incubated naive or 40LB culture system–induced in vitro GC (iGC) B cells with either OVA peptide ($OVA_{323–339}$), which can be loaded directly onto MHC-II, or a surrogate OVA antigen (anti-IgM-OVA conjugate), which must be internalized and processed in a BCR-dependent manner. We then co-cultured antigen-loaded WT or Cbl$^{-/-}$Cbl-b$^{-/-}$ B cells with CellTrace Violet (CTV)–labeled OT-II TCR Tg CD4$^+$ T (OT-II T) cells and measured their proliferation by flow cytometry. WT and Cbl$^{-/-}$Cbl-b$^{-/-}$ naive B cells loaded with $OVA_{323–339}$ peptide elicited a similar rate of OT-II T cell proliferation, indicating that naive WT and Cbl$^{-/-}$Cbl-b$^{-/-}$ B cells have a similar ability to present peptide antigen to T cells (Fig. 3 A). In contrast, while WT naive B cells processed intact anti-IgM-OVA antigen and presented it efficiently to T cells, as evidenced by the strong proliferation of co-cultured OT-II T cells, naive Cbl$^{-/-}$Cbl-b$^{-/-}$ B cells failed to induce OT-II T cell proliferation under the same condition. Efficiencies of OT-II T cell proliferation stimulated by WT and Cbl$^{-/-}$Cbl-b$^{-/-}$ iGC B cells loaded with either $OVA_{323–339}$ peptide or intact anti-IgM-OVA antigen were comparable and IgM expression was not reduced in Cbl$^{-/-}$Cbl-b$^{-/-}$ iGC B cells (Fig. S3, B and C), indicating that Cbls do not affect intact antigen uptake by IgM and antigen processing in iGC B cells. To further determine whether antigen presentation by in vivo–generated GC B cells required Cbls, we immunized Cbl$^{-/-}$Cbl-b$^{-/-}$ mice in which Cbls were deleted in GC B cells by the Ig Cγ-Cre allele, purified GC B cells by FACS sorting, and then examined their ability to present intact anti-IgM-OVA antigen to OT-II T cells. WT and mutant GC B cells loaded with either OVA peptides or the intact antigen induced equal amounts of OT-II T cell proliferation, thus indicating that Cbls are dispensable for the antigen processing by in vivo GC B cells (Fig. 3 B).

To determine whether lack of antigen presentation by naive Cbl$^{-/-}$Cbl-b$^{-/-}$ B cells affected their interaction with antigen specific T cells, we examined the ability of B cells to form T–B cell conjugates with cognate T cells in the presence of either peptide or intact antigen (Qi et al., 2008). We cultured OT-II T cells labeled with CTV (red) and WT or Cbl$^{-/-}$Cbl-b$^{-/-}$ B cells labeled with CFSE (green) in the presence of $OVA_{323–339}$ or anti-IgM-OVA antigen. CellTrace$^+$CFSE$^+$ T–B cell conjugates were examined by flow cytometry (Fig. 3, C and D). In the presence of $OVA_{323–339}$ peptide, naive WT and Cbl$^{-/-}$Cbl-b$^{-/-}$ B cells formed almost equal amounts of T–B cell conjugates with OT-II T cells. In contrast, naive Cbl$^{-/-}$Cbl-b$^{-/-}$ B cells formed significantly fewer T–B cell conjugates compared with WT B cells in the presence of anti-IgM-OVA antigen. To directly determine whether Cbl$^{-/-}$Cbl-b$^{-/-}$ B cells can express the processed antigenic peptide in MHC-II (pMHC-II) complexes, we stimulated WT and Cbl$^{-/-}$Cbl-b$^{-/-}$ naive or GC B cells with anti-IgM-Ea antigen in vitro and then examined Ea pMHC-II expressed by these cells with Y-Ae mAb. WT and Cbl$^{-/-}$Cbl-b$^{-/-}$ GC B cells were isolated from the immunized mice by FACS sorting. We found that after 3 h of stimulation, naive WT B cells expressed a significant high amount of Ea pMHC on the cell surface. In contrast, naive Cbl$^{-/-}$Cbl-b$^{-/-}$ B cells expressed almost no detectable Ea pMHC after the same stimulation (Fig. 3 E). Both WT and Cbl$^{-/-}$Cbl-b$^{-/-}$ GC B cells expressed significant and comparable amounts of Ea pMHC after anti-IgM-Ea stimulation (Fig. 3 E). To test whether Ea antigen could be processed in GC B cells in vivo, we immunized WT and Ig Cγ-Cre Cbl$^{-/-}$Cbl-b$^{-/-}$ mice with Ea-GFP and then examined Ea pMHC in GC B cells by FACS. We observed that WT and mutant GC B cells expressed a comparable level of Ea pMHC on the cell surface (Fig. S3 E), further indicating that antigen processing in GC B cells is not affected

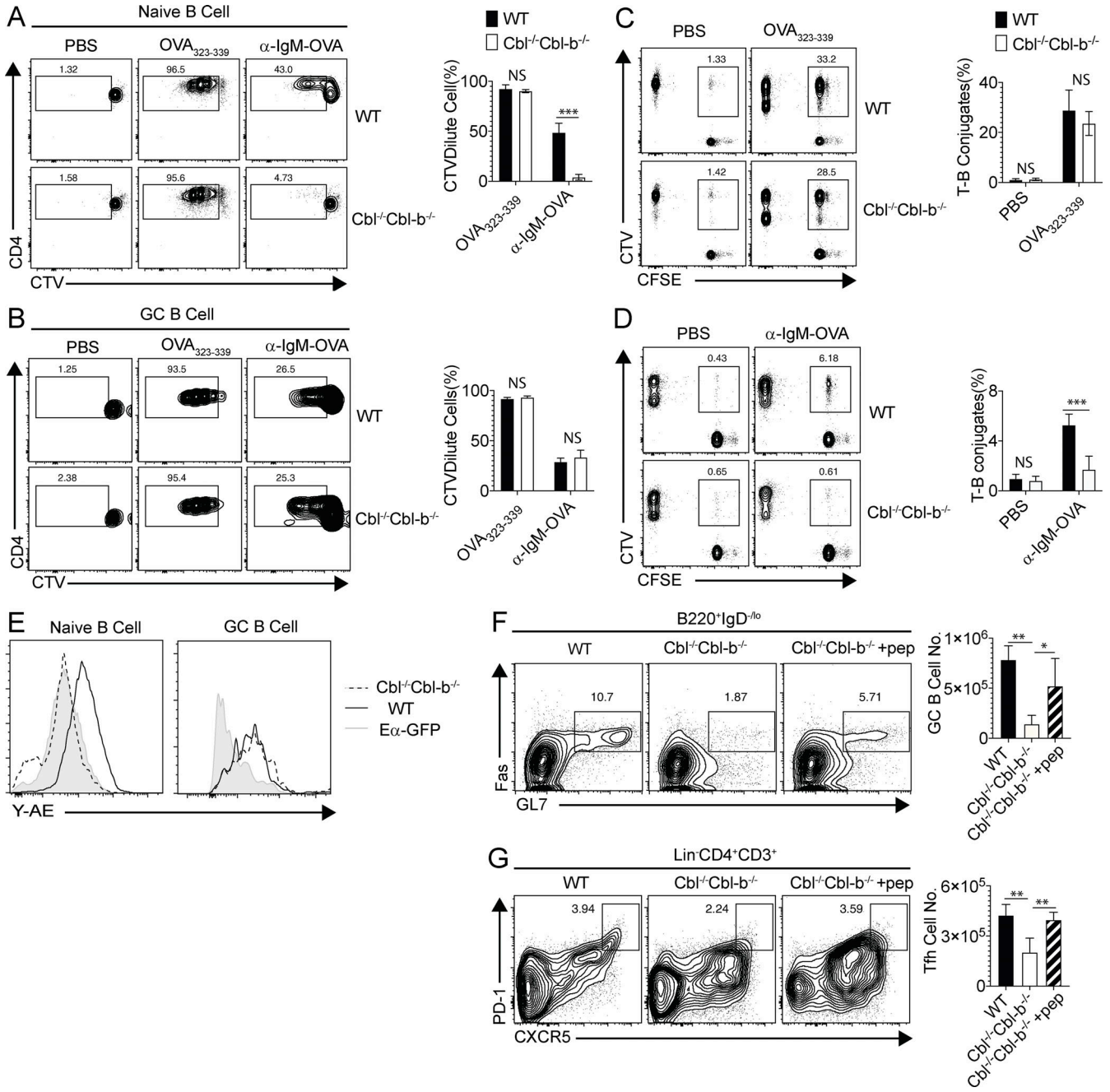

Figure 3. **Defective antigen presentation of naive Cbl$^{-/-}$Cbl-b$^{-/-}$ B cells to cognate T cells. (A)** OT-II T cell proliferation stimulated by $OVA_{323-339}$ peptide or anti-IgM-OVA–loaded naive B cells. Proliferation of OT-II T cells are measured based on the dilution of CTV fluorescent intensity. Shown are contour maps (left) of CTV intensity and statistics (right) of the gated OT-II T cells (n = 4). **(B)** OT-II T cell proliferation stimulated by $OVA_{323-339}$ peptide or anti-IgM-OVA loaded in vivo–generated GC B cells. Proliferation of OT-II T cells was measured based on the dilution of CTV fluorescent intensity. Shown are contour maps (left) of CTV intensity and statistics (right) of the gated OT-II T cells (n = 4). **(C and D)** Naive Cbl$^{-/-}$Cbl-b$^{-/-}$ B cells are deficient in cognate interaction with T cells upon anti-IgM-OVA stimulation. Naive WT or Cbl$^{-/-}$Cbl-b$^{-/-}$ B cells and OT-II T cells were labeled with CellTrace (red) and CFSE (green), respectively, and co-cultured in the presence of $OVA_{323-339}$ (C) or anti-IgM-OVA (D). 5 h later, T–B cell conjugates were analyzed by flow cytometry. Shown are FACS analyses (left) and statistics (right) of T–B cell conjugates in the culture (n = 4). **(E)** FACS analyses of ex vivo antigen presentation of $E\alpha_{52-68}$ peptide in naive B and GC B cells from WT and Cbl$^{-/-}$Cbl-b$^{-/-}$ mice. Shown are histogram comparisons of $E\alpha_{52-68}$ peptide on naive B (left) and GC B cells (right; n = 4). **(F and G)** Rescues of GC responses in Cbl$^{-/-}$Cbl-b$^{-/-}$ mice by peptide antigen. Shown are FACS analyses (left) and statistics of GC B (F) and Tfh (G) cells in WT or Cbl$^{-/-}$Cbl-b$^{-/-}$ mice with or without $OVA_{323-339}$ peptide injection (n = 4). Data are shown as means ± SD (A–G) and from at two independent experiments (B–D, F, and G) and three independent experiments (A and E). *, P < 0.05; **, P < 0.01; ***, P < 0.001 (A–E, unpaired Student's t test; F and G, one-way ANOVA multiple comparison test).

by Cbls. Together, these results demonstrate that Cbls play a pivotal role in controlling the capability of naive B cells to uptake and process intact antigen via the BCR. However, BCR-mediated antigen processing by GC B cells is independent of Cbls.

Impaired antigen processing by Cbl$^{-/-}$Cbl-b$^{-/-}$ B cells led us to question whether peptide antigen immunization could rescue GC responses in Cbl$^{-/-}$Cbl-b$^{-/-}$ mice. We therefore immunized mice with NP-OVA at day 0 and adoptively transferred OT-II TCR Tg CD4^{+} T cells to WT and Cbl$^{-/-}$Cbl-b$^{-/-}$ mice at day 1 to allow priming of antigen-specific B and T cells. We then injected the immunized mice with $OVA_{323-339}$ peptide at day 4 so it could be loaded into MHC-II of the B cells directly and analyzed GC B and Tfh cell development at day 10 by flow cytometry. Injection of $OVA_{323-339}$ peptide induced not only normal Tfh cell development but also significantly more GC B cells in the mutant mice (Fig. 3, F and G), suggesting that the defective Cbl$^{-/-}$Cbl-b$^{-/-}$ B cell antigen presentation can be rescued by the processed peptide antigen.

Together, our results show that naive B cells require Cbls to process and present antigen to and receive help from T cells. Since Cbl$^{-/-}$Cbl-b$^{-/-}$ GC B cells have a normal capability to present antigen to T cells, we propose that GC B cells may use a different mechanism to control BCR-mediated antigen uptake and processing than naive B cells. The latter result is also consistent with our previous finding that lack of Cbls in the in vivo GC B cells does not have a significant impact on the development of GC B cells (Li et al., 2018).

Cbls control BCR-mediated antigen endocytosis and postendocytic sorting to lysosomes

B cell antigen presentation involves multiple steps, including antigen capture by the BCR, internalization of BCR–antigen complexes, and intracellular sorting of the internalized BCR–antigen complexes to the lysosomal compartment for degradation (Avalos and Ploegh, 2014; Blum et al., 2013; Chaturvedi et al., 2011). To identify which of these steps was affected by the Cbl$^{-/-}$Cbl-b$^{-/-}$ mutation, we first examined IgM BCR internalization after BCR engagement by anti-IgM $(Fab)_2$. Anti-IgM $(Fab)_2$ stimulation induced rapid BCR internalization and downmodulation of >70% of cell surface BCRs in WT naive B cells within 15 min. In contrast, Cbl$^{-/-}$Cbl-b$^{-/-}$ naive B cells internalized 40% of cell surface IgM BCRs after the same period of stimulation (Fig. 4 A), indicating that BCR-mediated antigen internalization in naive B cells is partially compromised in the absence of Cbls. However, the rate of IgM BCR internalization in WT and Cbl$^{-/-}$Cbl-b$^{-/-}$ GC B cells generated in vivo was similar (Fig. 4 B), suggesting that Cbls do not affect BCR endocytosis in GC B cells. To determine whether the internalized BCR–antigen complexes were sorted to the late endosome/lysosome compartment for degradation and processing, we generated a lysosome degradation sensor described previously (Fig. S3 F; Nowosad et al., 2016). In this sensor, anti-IgM $(Fab)_2$ was conjugated to Atto647N and a quencher molecule that absorbs emission from Atto647N. Degradation of the sensor in acidic lysosomes relieves the quenching effect, resulting in emission of Atto647N fluorescence detectable by either flow cytometry or confocal microscopy. Quantification of Atto647N-positive cells by flow cytometry revealed that stimulation of WT naive B cells with the lysosome sensor for 10 min generated >60% of the Atto647N-positive cells, and this number increased to 70% after 30 min (Fig. 4 C). In contrast, Cbl$^{-/-}$Cbl-b$^{-/-}$ naive B cells produced less than 5% and 35% Atto647N positive cells, respectively, and the average intensity of the Atto647N signal in individual Atto647N $^{+}$ mutant naive B cells was significantly lower relative to WT controls. Degradation of the lysosome sensor in in vivo generated WT and Cbl$^{-/-}$Cbl-b$^{-/-}$ GC B cells was comparable (Fig. 4 D). Consistently, confocal microscopy revealed a significant amount of internalized BCR complexes (green) colocalized with Atto647N positive puncta in WT but not Cbl$^{-/-}$Cbl-b$^{-/-}$ naive B cells (Fig. 4 E). Lack of lysosomal sorting of the internalized BCR-antigen complexes in Cbl$^{-/-}$Cbl-b$^{-/-}$ B cells was further confirmed by analyzing the fraction of the internalized BCR colocalized with LAMP-1^{+} late endosomes/lysosomes by confocal microscopy (Fig. 4 F). In contrast, lysosome sorting of the internalized sensor in Cbl$^{-/-}$Cbl-b$^{-/-}$ iGC B cells was not affected as compared with WT control (Fig. S3 G). Based on these results, we conclude that Cbls not only control BCR-mediated antigen endocytosis but also post-endocytic trafficking to the lysosomes for degradation, and this regulation operates only in naive but not in vivo generated GC and iGC B cells.

Cbls control BCR-mediated endocytosis and postendocytic trafficking to lysosomes by ubiquitinating CD79A and CD79B

Membrane receptor internalization and trafficking to lysosomes can be regulated by ubiquitin signals (Piper et al., 2014). Since the BCR (IgM) has only a short (three amino acids) cytoplasmic tail and is constitutively associated with transmembrane proteins CD79A and CD79B (Reth, 1992), we examined whether Cbl proteins regulated BCR internalization and lysosomal trafficking by promoting CD79A and CD79B ubiquitination. We first stimulated BCR with anti-IgM $(Fab)_2$ and analyzed the ubiquitination status of CD79A and CD79B in naive or iGC B cells. Both CD79A and CD79B became polyubiquitinated in WT naive B cells. In contrast, ubiquitination of CD79A and CD79B in Cbl$^{-/-}$Cbl-b$^{-/-}$ naive B cells was almost completely blocked compared with WT controls (Fig. 5 A). Unlike in naive B cells, BCR stimulation did not change the ubiquitination status of CD79A and CD79B in WT or Cbl$^{-/-}$Cbl-b$^{-/-}$ iGC B cells as compared with nonstimulated cells (Fig. 5 B). iGC B cells were used for this assay, because we could not isolate enough in vivo GC B cells for the biochemical study. Together, these results show that Cbls are required for BCR-induced CD79A and CD79B ubiquitination in naive B cells. However, they are dispensable for the ubiquitin modification of CD79A and CD79B in activated iGC B cells.

Inspection of the protein sequences revealed three lysine residues in the cytoplasmic tails of both CD79A and CD79B, which may serve as putative ubiquitin accepting sites (Fig. S4 A). To determine whether ubiquitin modification of CD79A and CD79B was relevant to BCR-mediate antigen uptake and lysosome trafficking, we generated mutants of CD79A and CD79B in which all three lysines were replaced with arginines (termed CD79A$^{3K>R}$ and CD79B$^{3K>R}$, respectively; Fig. S4 A). These mutants were then introduced into hematopoietic stem cells from either CD79A$^{-/-}$ or CD79B$^{-/-}$ mice by retroviral expression

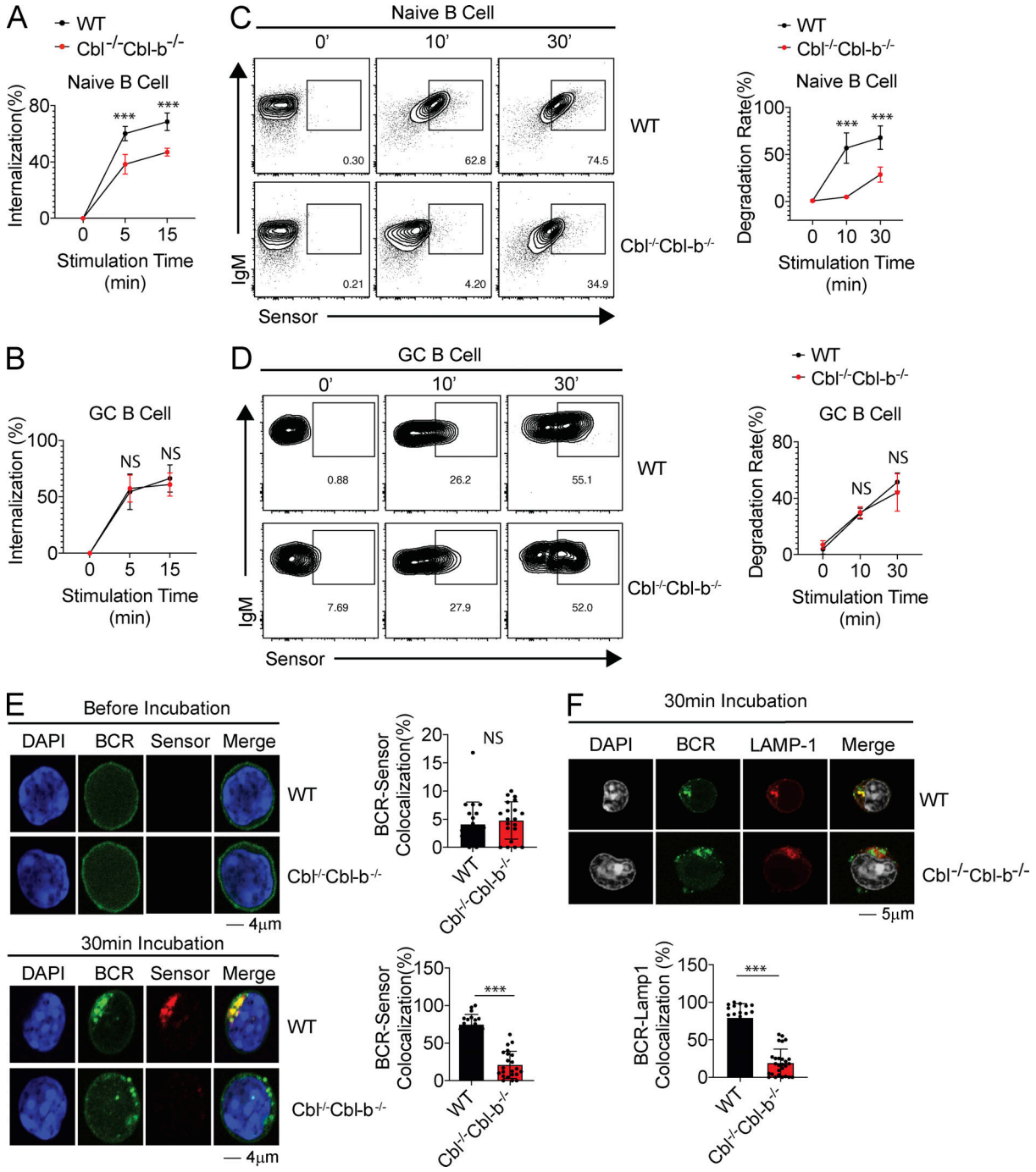

Figure 4. **Impaired BCR-mediated antigen endocytosis and postendocytic sorting to lysosomes by Cbl$^{-/-}$Cbl-b$^{-/-}$ B cells. (A and B)** FACS analyses of BCR downmodulation in Cbl$^{-/-}$Cbl-b$^{-/-}$ B cells. Naive B cells (A) or GC B cells (B) were stimulated with biotinylated anti-IgM (Fab)$_2$ for various periods. Cell surface remaining IgM was stained by streptavidin-FITC and quantified by FACS. Shown are the statistics of IgM downmodulation on WT and Cbl$^{-/-}$Cbl-b$^{-/-}$ naive (A) or GC (B) B cells (n = 3). **(C)** FACS analyses of BCR-mediated antigen degradation in naive B cells. Naive WT and Cbl$^{-/-}$Cbl-b$^{-/-}$ B cells were stimulated with the lysosome sensor for various times. Percentages of Atto647N$^+$ cells and the intensity of Atto647N signal in gated lysosome sensor degraded cells are determined by FACS analysis (n = 3). **(D)** FACS analyses of BCR-mediated antigen degradation in GC B cells. WT and Cbl$^{-/-}$Cbl-b$^{-/-}$ GC B cells were stimulated with the lysosome sensor for various times. Percentages of Atto647N$^+$ cells and the intensity of Atto647N signal in gated lysosome sensor degraded cells were determined by FACS analysis (n = 4). **(E)** Confocal microscopic analyses of BCR-endocytic trafficking. Shown are confocal microscopic images (left) of the BCR (green) vs. degraded lysosome sensor (red) and statistics (right) of BCR and lysosome colocalization before and after 30-min incubation at 37°C (n = 20). **(F)** Colocalization analysis of internalized BCR and lysosomes in Cbl$^{-/-}$Cbl-b$^{-/-}$ B cells. Shown are confocal images (left) of BCR (green) vs. Lamp-1 staining and statistics (right) of BCR and lysosome colocalization in naive B cells (n = 20). Data are shown as means ± SD (A–F) and from three independent experiments (A–D and E) and two independent experiments (F). ***, P < 0.001 (E and F, unpaired Student's t test; A–D, two-way ANOVA multiple comparison test).

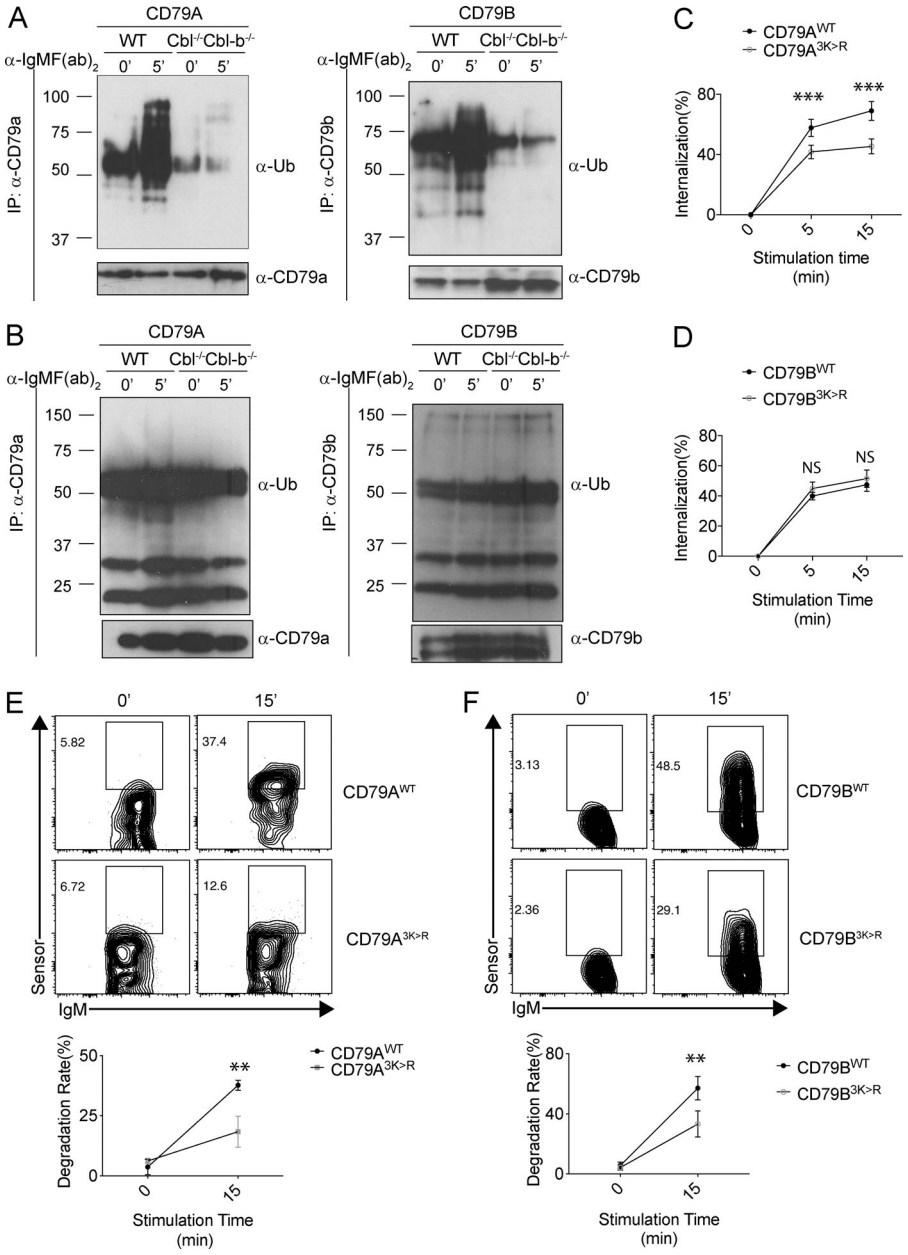

Figure 5. **Ubiquitination of CD79A and CD79B by Cbls and its relevance in BCR internalization and sorting to lysosomes. (A and B)** Ubiquitination (Ub) of CD79A and CD79B in naive and iGC B cells. Naive or in vitro iGC B cells from WT and Cbl$^{-/-}$Cbl-b$^{-/-}$ mice were stimulated with anti-IgM, respectively. Shown are the ubiquitination status of CD79A (left) and CD79B (right) in naive B cells (A) and iGC B cells (B), respectively (n = 2). IP, immunoprecipitation. **(C and D)** Blockade of CD79A but not CD79B ubiquitination reduces BCR downmodulation. Naive B cells expressing a WT or mutant CD79A (CD79A$^{3K>R}$) or CD79B (CD79B$^{3K>R}$) were stimulated with biotinylated anti-IgM (Fab)$_2$ for various periods. Cell surface remaining IgM were visualized by streptavidin-FITC staining. Shown are the statistics comparisons of cell surface IgM downmodulation in WT vs. CD79A$^{3K>R}$ (C) or WT vs. CD79B$^{3K>R}$ (D) B cells (n = 3). **(E and F)** Blockade of CD79A or CD79B ubiquitination attenuates internalized BCR trafficking to lysosomes. WT or CD79A$^{3K>R}$- or CD79B$^{3K>R}$-expressing B cells were stimulated with the lysosome degradation sensor. The percentage of cells with the sensor degradation (Alexa Fluor 647$^+$) was measured by FACS. Shown are FACS contour maps (top) and statistics (bottom) of lysosome sensor degradation in WT vs. CD79A$^{3K>R}$ (E) or WT vs. CD79B$^{3K>R}$ (F) B cells (n = 5). Data are shown as means ± SD and from two independent experiments (A–F). **, P < 0.01; ***, P < 0.001 (C–F, two-way ANOVA multiple comparison test).

vectors to generate BM chimeras, respectively. The retroviral vector expressing either a WT CD79A or CD79B was used as a control. We found that replacement of WT CD79A or CD79B with the mutant CD79A$^{3K>R}$ or CD79B$^{3K>R}$ did not significantly alter follicular B cell development, BCR expression, or signaling (Fig. S4, B–D). However, while BCR internalization in naive CD79B$^{3K>R}$-expressing B cells was not altered, it was partially blocked in CD79A$^{3K>R}$-expressing B cells, which was similar to our earlier results in Cbl$^{-/-}$Cbl-b$^{-/-}$ B cells (Fig. 5, C and D). To determine whether intracellular trafficking of the internalized BCR–antigen complexes was affected by CD79A and CD79B ubiquitination, we stimulated CD79A$^{3K>R}$ or CD79B$^{3K>R}$ naive B cells with the lysosome degradation sensor and examined the intracellular sensor degradation in lysosomes by flow cytometry. We found that both CD79A$^{3K>R}$- and CD79B$^{3K>R}$-expressing B cells exhibited a markedly reduced degradation of the internalized lysosome sensors relative to WT CD79A and CD79B-expressing B cells (Fig. 5, E and F). Taken together, our results support the conclusion that in naive B cells, CD79A ubiquitination is required for BCR internalization, whereas ubiquitination of CD79B is merely involved in the intracellular trafficking of the internalized BCR to the acidic endocytic compartment for degradation.

GC development depends on CD79A or CD79B ubiquitination and Cbls ubiquitin ligase activity

To determine whether CD79A and CD79B ubiquitination is relevant to GC development, we examined GC development in the above CD79A$^{3K>R}$ or CD79B$^{3K>R}$-BM chimeric mice after NP-KLH immunization. We found that WT CD79A- or CD79B-reconstituted BM chimeras produced high numbers of GC B cells, indicating that B cells reconstituted with WT CD79A- or

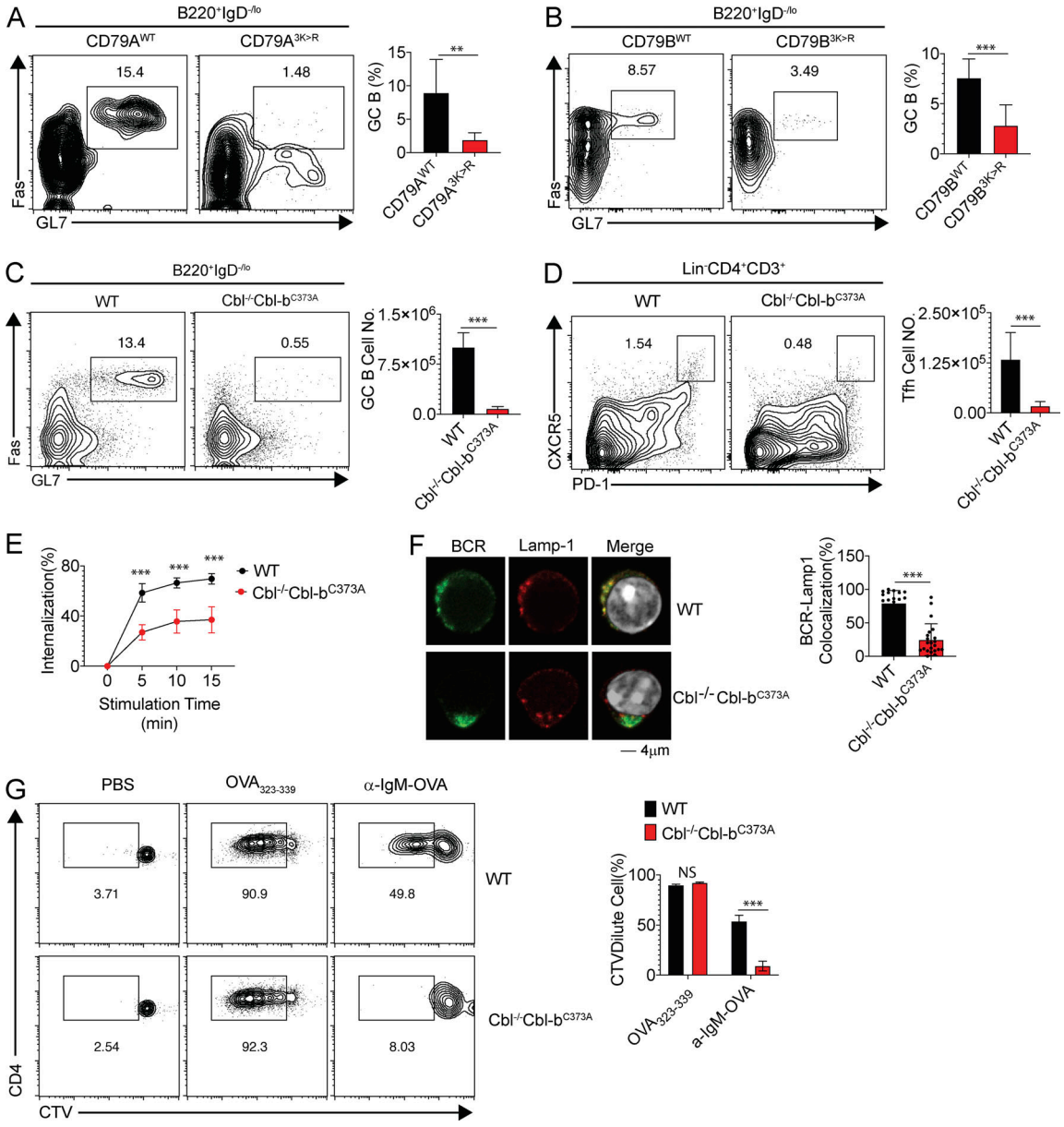

Figure 6. **Essential roles of Cbl ubiquitin ligase activity and CD79A or CD79B ubiquitination in GC reaction. (A and B)** Blockade of CD79A or CD79B ubiquitination impairs GC development. Shown are FACS contour maps (left) and statistics (right) of GC B cells in WT and CD79A$^{3K>R}$ (A) or WT and CD79B$^{3K>R}$ (B) BM chimeric mice after NP-KLH immunization, respectively (n = 5). **(C and D)** Inactivation of Cbl ubiquitin ligase activity impairs GC reaction. Shown are FACS contour maps (left) and statistics (right) of GC B cells (C) or Tfh cells (D) in NP-KLH immunized WT and Cbl$^{-/-}$Cbl-b^{C373A} mice (n = 5). **(E)** FACS analyses of BCR downmodulation in Cbl$^{-/-}$Cbl-b^{C373A} B cells. Naive B cells were stimulated with biotinylated anti-IgM (Fab)$_2$ for various periods. Cell surface remaining IgM was stained by streptavidin-FITC and quantified by FACS. Shown are the statistics of cell surface IgM dowmodulation of WT and Cbl$^{-/-}$Cbl-b^{C373A} naive B cells (n = 3). **(F)** Colocalization analysis of internalized BCR and lysosomes in Cbl$^{-/-}$Cbl-b^{C373A} B cells. Shown are confocal images (left) of BCR (green) vs. LAMP-1 (red) staining and statistical analysis (right) of BCR and lysosome colocalization in WT and Cbl$^{-/-}$Cbl-b^{C373A} naive B cells (n = 20). **(G)** OT-II T cell proliferation stimulated by OVA$_{323–339}$ peptide or anti-IgM-OVA loaded naive Cbl$^{-/-}$Cbl-b^{C373A} B cells. Proliferation of OT-II T cells are measured based on the dilution of CTV fluorescent intensity. Shown are contour maps (left) of CTV intensity and statistics (right) of the gated OT-II T cells (n = 4). Data are shown as means ± SD (A–G) and from two independent experiments (C–F) and three independent experiments (A, B, and G). **, P < 0.01; ***, P < 0.001. (B–D, F, and G, unpaired Student's t test; E, two-way ANOVA multiple comparison test).

CD79B-expressing retroviral vectors were functionally normal in terms of generating GC responses (Fig. 6, A and B). In contrast, mutant CD79A$^{3K>R}$- or CD79B$^{3K>R}$-expressing chimeras did not efficiently generate GC B cells (Fig. 6, A and B). This finding is thus consistent with our hypothesis that ubiquitination of CD79A and CD79B is necessary for the development of GC B cells.

Both Cbls may execute their regulatory roles through scaffolding and ubiquitin ligase functions (Li et al., 2018). Since Cbls promote CD79A and CD79B ubiquitination, we next decided to determine whether CBLs ubiquitin ligase activity was required for GC B and Tfh cell development. We generated *Cbl$^{Flox/Flox}$ Cbl-b$^{C373A/-}$ Mb1-Cre* Tg (termed Cbl$^{-/-}$Cbl-b^{C373A}) mice that

expressed a ligase activity–deficient Cbl-b^{C373A}, but not Cbl (Oksvold et al., 2008), and examined GC development after NP-KLH immunization. We found that Cbl$^{-/-}$Cbl-b^{C373A} mice had markedly reduced numbers of GC B cells and Tfh cells relative to WT counterparts (Fig. 6, C and D). Similar to Cbl$^{-/-}$Cbl-b$^{-/-}$ B cells, Cbl$^{-/-}$Cbl-b^{C373A} B cells could not efficiently internalize BCRs, sort the internalized BCR–antigen complexes to lysosomes, or present antigen to T cells (Fig. 6, E–G). These results thus indicate that the phenotypes of the defective GC development found in Cbl$^{-/-}$Cbl-b$^{-/-}$ mice can be attributed to the lack of Cbl ubiquitin ligase activity.

Cbl$^{-/-}$Cbl-b$^{-/-}$ mice fail to generate protective humoral immunity to intestinal helminth infection

Antigen uptake by B cells during pathogen infection is complicated not only by the route through which pathogen-derived antigens reach B cells but also by their widely diverse epitopes that may have a broad range of affinities to BCRs. To determine whether the complex antigenicity of pathogens could enable B cells to bypass Cbl-regulated antigen uptake and enter the GC reaction, we examined GC responses following infection with the intestinal parasitic helminth *Heligmosomoides polygyrus bakeri* (*Hpb*; Meli et al., 2016). We found that *Hpb* infection induced significantly reduced numbers of GC B cells and Tfh cells in both the draining mesenteric LNs and spleens of Cbl$^{-/-}$Cbl-b$^{-/-}$ mice relative to WT controls (Fig. 7, A and B). The mutant mice also produced significantly lower titers of serum anti-*Hpb* IgG1 (Fig. 7 C) and exhibited significantly higher egg counts and worm burden relative to WT mice upon secondary infection (Fig. 7, D and E). These data indicate that Cbls also control protective humoral immunity to a complex parasite, likely by facilitating helminth-derived antigen uptake and processing in B cells.

Discussion

BCR-mediated antigen uptake and processing play a critical role in the cognate interaction of B and T cells. Although a significant amount of evidence indicates that T–B cell cognate recognition is required for the initial entry of antigen-specific B cells into the GC reaction (Shulman et al., 2014; Victora and Nussenzweig, 2012), selection of BCR affinity, and differentiation of GC B cells into PCs or memory B cells, the molecular mechanisms underlying this regulation are not yet clear. Our study provides clear evidence showing that Cbls are essential regulators of naive B cell antigen uptake and presentation by facilitating BCR-mediated antigen endocytosis and postendocytic sorting to lysosomes for degradation. In the absence of B cell–intrinsic Cbls, the GC reaction cannot be initiated due to the impairment in B cell priming of naive T cells into Tfh cells and cognate T–B cell interaction. While naive T and Tfh cell activation might have different thresholds in response to antigen stimulation, our observation that even a high dose of SRBC or a complex antigen such as parasitic helminth infection could not generate effective GC and antibody responses suggests that the failure to generate GCs is less likely a result of limited availability of antigens to activate naive T cells in vivo. Taken together, our study suggests that Cbls are an indispensable central player in B cell antigen uptake and processing at the entry checkpoint of the GC reaction.

Receptor endocytosis and postendocytic trafficking to lysosomes generally involves multiple mechanisms, including clathrin-coated pit formation, receptor ubiquitination, cytoskeleton reorganization, and coordinated receptor signaling. While previous studies have shown that B cells may also employ these mechanisms for BCR internalization (Avalos and Ploegh, 2014; Blum et al., 2013; Chaturvedi et al., 2011; Jacob et al., 2008; Veselits et al., 2017), there was no evidence that antibody responses and the GC reaction require these molecular events. Our studies using Cbl$^{-/-}$Cbl-b$^{-/-}$ B cells provide clear data that ubiquitination of CD79A and CD79B in BCR complexes by Cbls is necessary for the initiation of the GC reaction and T cell–dependent antibody responses in vivo. In particular, Cbls promote the ubiquitination of both CD79A and CD79B in naive B cells, and these ubiquitination events are required for BCR-mediated antigen uptake, processing, and eventually the T–B cell interactions necessary for humoral immunity to protein antigen immunization or parasite infection. While blockade of CD79A ubiquitination attenuates BCR-mediated antigen endocytosis, blockade of CD79B ubiquitination only affects the intracellular trafficking of the internalized BCR to the acidic LAMP-1^{+} late endosome/lysosome compartment for degradation. Therefore, our findings not only establish the importance of Cbl-mediated BCR ubiquitination in B cell antigen processing and presentation, T–B cell cognate interactions, and initiation of the GC reaction but also reveal that ubiquitination of CD79A and CD79B may act at different checkpoints of the BCR endocytic and postendocytic trafficking cascade during antigen processing in naive B cells. Development of tools to target these checkpoints may help to boost antibody responses for vaccination or suppress GC responses for the treatment of autoimmune diseases in the future. It should be noted that Cbls might also have different targets at different stage of B cell development, as we have found that expression of IRF4, a target of Cbls in GC B cells (Li et al., 2018), is not affected by Cbl deficiency in naive B cells (Fig. S4 E). How can Cbls exert such selective regulatory function at different stages of B cell development is another challenging question to address in the future.

Our finding that Cbls promote BCR-mediated antigen uptake and processing in naive, but not activated, GC B cells may be of fundamental importance for the overall regulation of the GC response. BCRs expressed by naive B cells contain germline VH and VL genes, which encode diverse, often low-affinity BCRs to the encounter antigens. It is therefore envisioned that in order to recruit more antigen-specific B cells with diverse repertoire into the GC reaction, naive B cells, including those expressing a low-affinity BCR, must employ an efficient mechanism to uptake sufficient antigen to receive productive Tfh cell help. The affinity of BCRs can be subsequently increased in GCs via SHM and clonal selection. In contrast to naive B cells, BCRs expressed by GC B cells have a much broader range of affinity/avidity toward antigens. In this case, a less efficient antigen uptake mechanism may help to discriminate BCR affinity, consequently favoring B cells with a high-affinity BCR to capture sufficient antigen and receive continued T cell help. Consistent with this

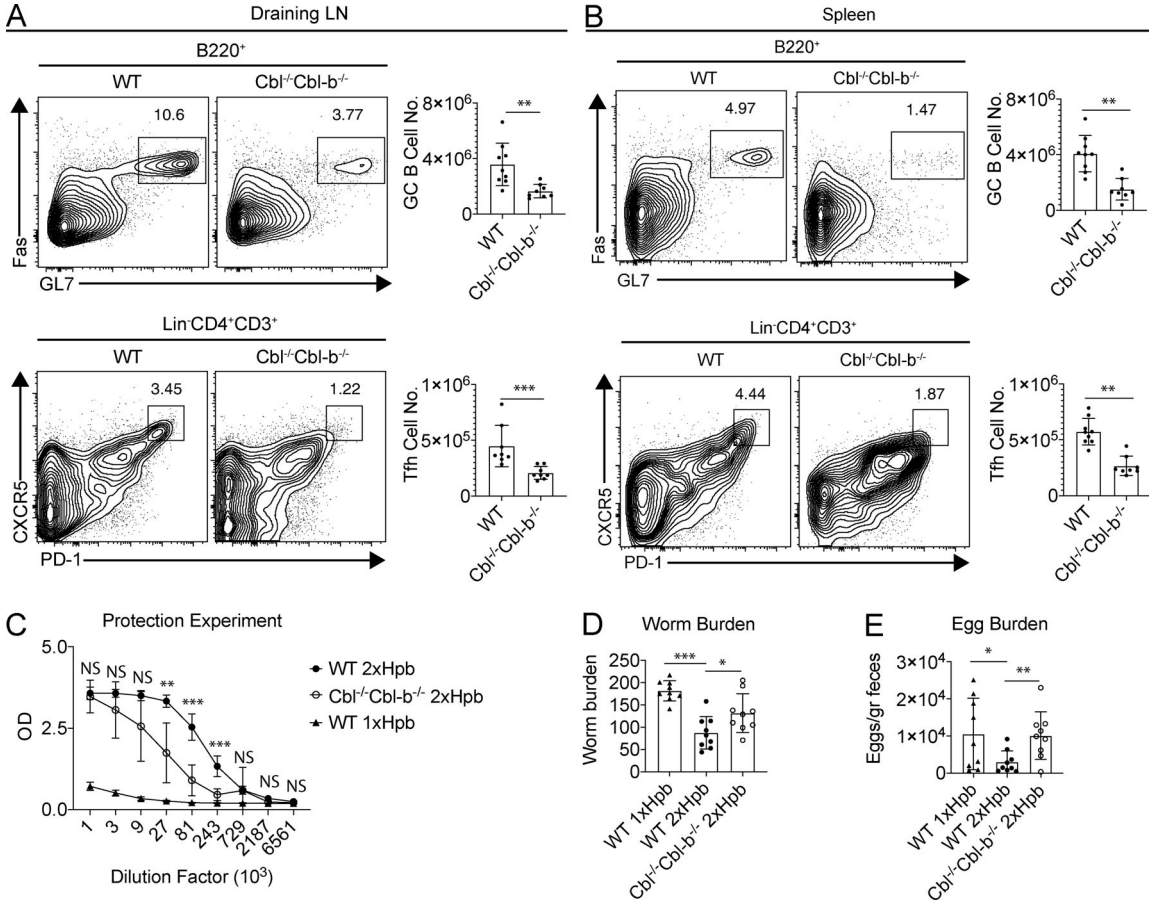

Figure 7. **Cbl$^{-/-}$Cbl-b$^{-/-}$ mice are deficient in mounting anti-helminth antibody responses. (A and B)** Reduced GC B and Tfh cells in Cbl$^{-/-}$Cbl-b$^{-/-}$ mice relative to WT controls after *Hpb* infection. Shown are FACS contour maps of GC B cells (top panel) and Tfh cells (bottom panel) from draining LNs (A) and spleen (B) of *Hpb*-infected WT and Cbl$^{-/-}$Cbl-b$^{-/-}$ mice (n = 8). **(C)** ELISA analysis of serum titers of anti-*Hpb* IgG1 after *Hpb* challenge (n = 9). **(D)** Egg counts/gram of feces from *Hpb* infected mice after *Hpb* challenge (n = 9). **(E)** Worm load (worms/mouse) in *Hpb*-infected mice after *Hpb* challenge (n = 9). Data are shown as means ± SD (A, B, D, and E) and are pooled results from two independent experiments; data in C are representative of two independent experiments with at least four mice/group for each experiment. *, P < 0.05; **, P < 0.01; ***, P < 0.001 (A and B, unpaired Student's t test; C–E, one-way ANOVA multiple comparison test).

view, recent studies have shown that naive B cells efficiently internalize antigen irrespective of their BCR affinity, whereas for GC B cells, only high-affinity B cells internalize antigen efficiently (Kwak et al., 2018; Nowosad et al., 2016). Since our studies demonstrate that Cbls-enhanced antigen uptake and processing occurs in naive, but not GC, B cells, we propose that by enforcing BCR-mediated antigen endocytic and postendocytic sorting in naive B cells, Cbls establish an efficient way to enable naive B cells with a broad range of BCR affinities into the GC reaction. This would increase the diversity of the initial repertoire of antigen-specific B cells whose affinity can be subsequently improved through the GC reaction.

Our studies also show that Cbls do not promote CD79A and CD79B ubiquitination in iGC B cells, suggesting that in vivo GC B cells may use different mechanisms to control BCR-mediated antigen uptake and processing. Consistent with this notion, we have previously reported that ablation of Cbls in in vivo GC B cells using the Ig-Cγ-Cre allele imposes only moderate effect on the total number of GC B cells (Li et al., 2018). However, our findings reveal that ubiquitination of CD79A and CD79B is not altered in iGC B cells irrespective of BCR stimulation, suggesting that a similar modification may operate in activated B cells, including in vivo GC B cells. The functional significance of these distinctively modified CD79A and CD79B molecules remains unclear. It will be interesting to determine whether other ubiquitin ligases are responsible for these ubiquitin modifications in GC B cells and whether such modifications play any role in GC B cell antigen uptake and processing. A model that conditionally expresses an ubiquitination-disabled CD79A or CD79B after B cells enter the GC stage may help to address this question.

In our previous study, we have shown that both Cbls are highly expressed in GC B cells as compared with naive B cells (Li et al., 2018). It is therefore unclear why Cbls do not promote CD79A and CD79B ubiquitination in GC B cells. One possible explanation is that Cbls are not directly associated with CD79A and CD79B in GC B cells and require other adaptors to function. Consistent with this possibility, it has been reported that the tyrosine kinase Syk can function as a scaffold for BCR and Cbl-b (Katkere et al., 2012). Alternatively, it is possible that Cbls

association with the BCR requires additional posttranslational modifications, such as Cbl phosphorylation, that may be differentially regulated in naive and GC B cells. Identification of these modifications may bring new insight into the BCR-regulated pathways in the GC reaction and antibody production in the context of human diseases.

Materials and methods

Animals

C57BL/6 mice, B6.SJL mice, OT-II TCR Tg mice, and Rag1$^{-/-}$ mice were purchased from The Jackson Laboratory. *Cbl*$^{flox/flox}$ and *Cbl-b*$^{-/-}$ mice were described previously (Li et al., 2018). To generate Cbl$^{-/-}$Cbl-b$^{-/-}$ mice, *Cbl*$^{flox/flox}$ and *Cbl-b*$^{-/-}$ mice were crossed to *Mb1-Cre* Tg mice kindly provided by Professor Michael Reth (Max Planck Institute of Immunology and Epigenetics, Freiburg, Germany). Cbl-b^{C373A} mice were described previously (Li et al., 2018). To obtain Cbl$^{-/-}$Cbl-b$^{-/-}$ GC B cells, *Cbl*$^{flox/flox}$ and *Cbl-b*$^{-/-}$ mice were crossed to *Cgamma1-Cre* Tg mice kindly provided by Professor Klaus Rajewsky (Max Delbruck Center for Molecular Medicine, Berlin, Germany). IL21^{Kat}IL4^{GFP} dual report mice were kindly provided by Professor J. Craft (Yale School of Medicine, New Haven, CT; Weinstein et al., 2016). To generate CD79A knockout mice, *Mb1-Cre* Tg mice were intercrossed to generate homozygous mice in which CD79A is disrupted by the *Cre Tg*. CD79B knockout mice were generated using a CRISPR-Cas9 method in the Institut de Recherches Cliniques de Montreal animal facility using the guide RNAs (gRNAs) listed in Table S1. In-house–generated mouse strains, including CD79A$^{-/-}$, CD79B$^{-/-}$, and Cbl$^{-/-}$Cbl-b$^{-/-}$, were on a C57BL/6 background. Both WT C57BL/6 mice and *Mb1-Cre tg* mice were used as control. All animal experiments were done in accordance with the Canadian Council of Animal Care and approved by the Institut de Recherches Cliniques de Montreal Animal Care Committee.

Plasmids, cell lines, and culture

cDNA encoding CD79A^{WT} and CD79B^{WT} was amplified by PCR and cloned into the MSCV-MIGR-GFP retroviral vector. To generate the three point mutations from lysine to arginine (3K>R) in CD79A and CD79B, PCR-assisted mutagenesis was performed using the different primer combinations listed in Table S1. CD79A$^{3K>R}$ and CD79B$^{3K>R}$ mutations were confirmed by DNA sequencing. Retroviruses were prepared according to our previous publication (Li et al., 2018). For iGC B cell culture, purified naive B cells were plated on 40LB feeder cells and cultured as described previously (Li et al., 2018).

Immunization, cell transfer, and helminth infection

For T cell–independent antibody responses, 6- to 10-wk-old mice were immunized with 50 µg type-I T cell–independent antigen NP-LPS precipitated in alum adjuvant by i.p. injection. Serum samples were collected at 7 d after immunization. For T cell–dependent antibody responses and quantification of GC reaction, mice were immunized with either 10^9 SRBCs in PBS or 50 µg of NP_{16}-OVA or NP_{36}-KLH precipitated in alum adjuvant by i.p. injection. Mice were analyzed at different time points after immunization. For the adaptive transfer, 1×10^6 of CD4$^+$ T cells purified from OT-II Tg mice were adoptively transferred into recipient mice by IV injection 1 d before immunization. Mice were then immunized with NP-OVA according to above.

Hpb infection was performed by gavage of 200 L3 *Hpb* larvae. Infected mice were sacrificed, mesenteric LNs and spleens were harvested, and single cell suspensions were prepared and subjected to FACS analysis at 2 wk after infection. For protection experiments, adult *Hpb* were eliminated at 4 wk after infection by two doses of pyrantel at 100 mg/kg administered by gavage 2 d apart. 2 wk later, cured mice were orally challenged with 200 larvae as previously described (Meli et al., 2016). Adult worm burden and egg counts were assessed 2 wk after rechallenge.

Flow cytometry

To examine the expression of cell surface markers, splenic or draining LN cells or purified B cells were resuspended in FACS buffer (5% BSA in PBS with 0.05% sodium azide), stained with corresponding antibodies on ice for 30 min, and then analyzed on a FACS BD Fortessa or Cyan. To analyze nuclear protein BCL6, splenic cells were first stained with corresponding antibodies, fixed and permeabilized with BD fix/Perm kit according to the manufacturer's instruction, and then stained with anti-BCL6. A list of antibodies used in this study is provided in Table S2.

Immunofluorescence

Spleens from either unimmunized mice or NP_{36}-KLH immunized mice were harvested and then embedded in optimum cutting temperature compound and flash-frozen in liquid nitrogen. Tissue sections were cut on a cryotome and fixed in ice-cold acetone. Sections were blocked with 5% BSA in PBS for 1 h at room temperature and stained with anti-CD35, anti-B220, peanut agglutinin, anti-CD3, anti-IgD, anti-CD1d, and anti-SIGN-R1 in various combinations. The following secondary antibodies were used: Streptavidin–Alexa Fluor 488 and Streptavidin–Alexa Fluor 633. Confocal images were acquired on a Zeiss LSM700 or 710.

To visualize BCR-mediated antigen degradation, purified B cells or 40LB-cultured iGC B cells were stimulated with the lysosome sensor for different time periods (0 and 30 min). Cells were transferred to glass slides using a cytospin, fixed at room temperature, and mounted with DAPI. Images were acquired on a Zeiss LSM710. To quantify BCR–antigen complex degradation in lysosomes, naive or iGC B cells were incubated with anti-IgM $F(ab)_2$-biotin on ice for 30 min. After removing the unbound antibody, samples were incubated at 37°C for different time periods (0 and 30 min) and then transferred to glass slides by cytospin. After fixation and permeabilization with 2% paraformaldehyde (PFA) and 0.1% Triton X-100, cells were stained with anti-LAMP-1 followed by anti-rabbit Alexa Fluor 568 and streptavidin Alexa Fluor 488. Images of LAMP-1 and BCR co-localization were acquired on a Zeiss LSM710.

Enzyme-linked immunospot assay and ELISA

Splenic cells from NP_{36}-KLH immunized mice were cultured in a NP_4-BSA– or NP_{30}-BSA–coated 96-well multiscreen-HA filter plate at 37°C overnight. IgG1 antibody–secreting cells were detected by staining with HRP-conjugated rabbit anti-mouse IgG1

and visualized by AEC substrate (BD PharMingen). The IgG1-positive spots were counted on a dissecting microscope. Anti-NP ELISAs were performed as previously described (Li et al., 2018). To detect parasite-specific IgG1, 96-well flat-bottom plates were coated with 1 µg/ml *Hpb* excretory/secretory proteins and incubated at 4°C overnight. Plates were washed, and serially diluted serum samples were added followed by incubation with rat anti-mouse IgG1-Biotin (SB77E) and streptavidin-HRP (Southern Biotech).

T–B cell co-culture

To evaluate the antigen-presentation capability of naive B and GC B cells, two types of antigen were used: $OVA_{323–339}$ peptide and anti-IgM-OVA surrogate antigen. To generate the surrogate antigen anti-IgM $F(ab)_2$-biotin, OVA-biotin, and streptavidin were mixed at a 4:4:1 ratio and incubated at room temperature for 30 min. The purified naive B cells or GC B cells were pretreated with either OVA peptide or surrogate antigen for 30 min at 37°C. After three washes to remove unbound antigens, samples were co-cultured with CTV-labeled OT-II $CD4^+$ T cells at a 1:2 ratio at 37°C for 48 or 72 h. OTII T cell proliferation was determined by FACS based on CTV intensity.

T–B cell conjugation assay

The T–B cell conjugation assay was performed and modified based on previous publication (Qi et al., 2008). In brief, purified OT-II $CD4^+$ T cells and naive B cells were labeled with CellTrace and CFSE, respectively. Labeled OT-II T cells and B cells were co-cultured with either $OVA_{323–339}$ peptide or anti-IgM-OVA surrogate antigen in a 96-well U-bottom plate at 37°C for 5 h. T–B cell conjugates identified as $CellTrace^+CFSE^+$ double-positive cells were quantified by flow cytometry.

In vivo and ex vivo antigen presentation assay

To test ex vivo antigen processing, purified naive and GC B cells were incubated with 10 µg/ml anti-IgM-Eα-GFP, Eα-GFP for 3 h at 37°C. Surface Eα pMHC-II was detected by staining the naive and GC B cells with biotin-conjugated Y-Ae mAb (Thermo Fisher) antibody. To access the in vivo antigen-presentation capability of GC B cells, mice were immunized with Eα-GFP. GC B cells were purified from Eα-GFP immunized mice. The surface expression level of Eα peptide on MHC-II was determined by Y-AE antibody.

BCR downmodulation assay

Freshly purified naive B, GC B, or iGC B cells were incubated with 10 µg/ml anti-IgM $F(ab)_2$-biotin for 30 min on ice. Unbound antibodies were removed by washing with PBS twice. Cells were then cultured at 37°C for various periods of time (0, 5, and 15 min) to allow BCR internalization to occur. The reaction was stopped by adding 2% PFA. Cell surface remaining BCR was stained with streptavidin-PE-CY7 and analyzed on a FACS.

BCR-mediated antigen degradation

The lysosomal degradation sensor was prepared according to a previous publication (Nowosad et al., 2016), and the DNA sequence of this sensor is listed in Table S1. To test BCR-mediated antigen uptake and degradation, purified naive B cells, GC B cells, or iGC B cells were incubated with the degradation sensor on ice for 30 min. After washing three times with PBS, cells were cultured at 37°C for various periods of time (0, 10, and 30 min) to allow BCR endocytosis and intracellular transport to lysosomes to occur. 2% PFA PBS solution was then added to stop the reaction. The rate of antigen degradation was quantified by FACS and confocal microscopy.

Immunoprecipitation and immunoblotting

Naive or iGC B cells were stimulated with anti-IgM $(Fab)_2$ at 37°C for 5 min. Cell lysates were first incubated with protein G agarose at 4°C for 1 h to remove mouse IgG produced by PCs. CD79A or CD79B protein in cell lysates was immunoprecipitated by incubation with 1 µg/ml of the corresponding antibodies at 4°C overnight, followed by incubation with protein G agarose at 4°C for another 1 h. Immunoprecipitates were washed with Tris-NaCl-EDTA buffer and immunoblotted to a polyvinylidene difluoride membrane. The following antibodies were used for Western blot hybridization: anti-IgM $F(ab)_2$, anti-CBL, anti-CBL-B, anti-β actin, anti-CD79A, anti-CD79B, and anti-ubiquitin antibody. Horseradish-peroxidase-conjugated goat anti-rabbit, goat anti-mouse, or donkey anti-goat antibodies were used as secondary antibodies. Images on the membranes were developed with an enhanced chemiluminescence detection system (GE Healthcare).

Generation of BM chimeric mice

To generate 50:50 BM chimeric mice, 8- to 10-wk-old recipient $Rag1^{-/-}$ mice were lethally irradiated (9.5 Gy). On the same day, total BM cells (4×10^6 cells/mouse) from B6.SJL and C57BL/6 or $Cbl^{-/-}Cbl\text{-}b^{-/-}$ mice were mixed at 1:1 ratio and transplanted into the recipient mice by i.v. injection. 6–8 wk after the transfer, BM chimeric mice were immunized with SRBCs by i.v. injection and analyzed according to the method described above.

To generate $CD79A^{WT}$, $CD79A^{3K>R}$, $CD79B^{WT}$, and $CD79B^{3K>R}$ BM chimeric mice, retroviral stocks were prepared according to our previous publication (Li et al., 2018). In brief, viral supernatants were collected 48 and 72 h after the transfection. To obtain BM stem cells, $CD79A^{-/-}$ mice and $CD79B^{-/-}$ mice were treated with 5-fluorouracil (5-FU; 5 mg/mouse, i.p.). 4 d later, BM stem cells were collected and cultured under optimal stem cell culture condition. After two rounds of retrovirus spin infection, virus-infected BM cells were collected and transferred into lethally irradiated (9.5 Gy) $Rag1^{-/-}$ recipient mice. 6 wk later, mice were immunized with NP_{36}-KLH and analyzed 7–10 d after immunization.

Statistical analysis

Statistical analyses were performed with a two-tailed, unpaired Student's *t* test, Mann–Whitney test, two-way ANOVA, or one-way ANOVA multiple comparison test with the assumption of equal sample variance, with GraphPad Prism V7 software. A P value <0.05 was considered as statistically significant.

Online supplemental material

Fig. S1 provides characterization of general B cell development and T cell–independent immune response in $Cbl^{-/-}Cbl\text{-}b^{-/-}$

mice. Fig. S2 provides additional characterization of Tfh and GC B cell phenotypes in Cbl$^{-/-}$Cbl-b$^{-/-}$ mice. Fig. S3 provides additional results showing how Cbls control BCR downmodulation and intracellular trafficking in naive B cells, but not GC B and iGC B cells. Fig. S4 provides characterization of B cell development and BCR signaling in CD79A$^{3K>R}$ and CD79B$^{3K>R}$ mice. Table S1 lists the primers and gRNA used in this study. Table S2 lists the antibodies used for flow cytometry.

Acknowledgments

We thank P. Tolar (The Francis Crick Institute, London, England) for the protocol for preparing the lysosomal degradation sensor, S. Pierce (National Institute of Allergy and Infectious Diseases, Bethesda, MD) for the anti-CD79A antibody, D. Kitamura (Tokyo University of Science, Noda, Japan) for the 40LB cells, J. Craft (Yale School of Medicine, New Haven, CT) for the IL4^{GFP}IL-21^{Kat} mice, O. Bannard (MRC Weatherall Institute of Molecular Medicine, Oxford, England) and J. Cyster (University of California, San Francisco, San Francisco, CA) for Eα-GFP construct and related information, and K. Rajewsky and A. Veillette for critical reading of the manuscript.

This work was supported by Canadian Institutes of Health Research operating grant MOP142279 and A. Aisenstadt Chair Fund to H. Gu, Chinese Scholarship Council PhD training grants to X. Li and W. Sun, a Cole Foundation postdoctoral fellowship to X. Li, Fonds de recherché du Quebec doctoral fellowships to A.P. Meli, Canadian Institutes of Health Research operating grant MOP130579 and Canada Research Chair in Barrier Immunity to I.L. King, and a Feinstein Institute for Medical Research institutional grant to Y.R. Zou.

Author contributions: X. Li did mouse, biochemical, and flow cytometric analyses. L. Gong and W. Sun contributed to some mouse, flow cytometric, and biochemical studies. A.P. Meli, D. Karo-Atar, and I.L. King contributed to *Hpb* infection studies, and I.L. King contributed to discussion. Y.R. Zou contributed to part of the immunofluorescent staining studies. Y.R. Zou and H. Gu contributed to experimental design and manuscript writing. All authors had editorial input.

Disclosures: The authors declare no competing interests exist.

Submitted: 16 August 2019
Revised: 19 March 2020
Accepted: 4 May 2020

References

Allen, C.D., T. Okada, and J.G. Cyster. 2007. Germinal-center organization and cellular dynamics. *Immunity*. 27:190–202. https://doi.org/10.1016/j.immuni.2007.07.009

Avalos, A.M., and H.L. Ploegh. 2014. Early BCR Events and Antigen Capture, Processing, and Loading on MHC Class II on B Cells. *Front. Immunol.* 5: 92. https://doi.org/10.3389/fimmu.2014.00092

Batista, F.D., and N.E. Harwood. 2009. The who, how and where of antigen presentation to B cells. *Nat. Rev. Immunol.* 9:15–27. https://doi.org/10.1038/nri2454

Blum, J.S., P.A. Wearsch, and P. Cresswell. 2013. Pathways of antigen processing. *Annu. Rev. Immunol.* 31:443–473. https://doi.org/10.1146/annurev-immunol-032712-095910

Chaturvedi, A., R. Martz, D. Dorward, M. Waisberg, and S.K. Pierce. 2011. Endocytosed BCRs sequentially regulate MAPK and Akt signaling pathways from intracellular compartments. *Nat. Immunol.* 12:1119–1126. https://doi.org/10.1038/ni.2116

Choi, Y.S., R. Kageyama, D. Eto, T.C. Escobar, R.J. Johnston, L. Monticelli, C. Lao, and S. Crotty. 2011. ICOS receptor instructs T follicular helper cell versus effector cell differentiation via induction of the transcriptional repressor Bcl6. *Immunity*. 34:932–946. https://doi.org/10.1016/j.immuni.2011.03.023

Crotty, S.. 2011. Follicular helper CD4 T cells (TFH). *Annu. Rev. Immunol.* 29: 621–663. https://doi.org/10.1146/annurev-immunol-031210-101400

De Silva, N.S., and U. Klein. 2015. Dynamics of B cells in germinal centres. *Nat. Rev. Immunol.* 15:137–148. https://doi.org/10.1038/nri3804

Gitlin, A.D., Z. Shulman, and M.C. Nussenzweig. 2014. Clonal selection in the germinal centre by regulated proliferation and hypermutation. *Nature*. 509:637–640. https://doi.org/10.1038/nature13300

Huang, F., and H. Gu. 2008. Negative regulation of lymphocyte development and function by the Cbl family of proteins. *Immunol. Rev.* 224:229–238. https://doi.org/10.1111/j.1600-065X.2008.00655.x

Jacob, J., G. Kelsoe, K. Rajewsky, and U. Weiss. 1991. Intraclonal generation of antibody mutants in germinal centres. *Nature*. 354:389–392. https://doi.org/10.1038/354389a0

Jacob, M., L. Todd, M.F. Sampson, and E. Puré. 2008. Dual role of Cbl links critical events in BCR endocytosis. *Int. Immunol.* 20:485–497. https://doi.org/10.1093/intimm/dxn010

Jang, I.K., D.G. Cronshaw, L.K. Xie, G. Fang, J. Zhang, H. Oh, Y.X. Fu, H. Gu, and Y. Zou. 2011. Growth-factor receptor-bound protein-2 (Grb2) signaling in B cells controls lymphoid follicle organization and germinal center reaction. *Proc. Natl. Acad. Sci. USA*. 108:7926–7931. https://doi.org/10.1073/pnas.1016451108

Katkere, B., S. Rosa, and J.R. Drake. 2012. The Syk-binding ubiquitin ligase c-Cbl mediates signaling-dependent B cell receptor ubiquitination and B cell receptor-mediated antigen processing and presentation. *J. Biol. Chem.* 287:16636–16644. https://doi.org/10.1074/jbc.M112.357640

Khalil, A.M., J.C. Cambier, and M.J. Shlomchik. 2012. B cell receptor signal transduction in the GC is short-circuited by high phosphatase activity. *Science*. 336:1178–1181. https://doi.org/10.1126/science.1213368

Kitaura, Y., I.K. Jang, Y. Wang, Y.C. Han, T. Inazu, E.J. Cadera, M. Schlissel, R.R. Hardy, and H. Gu. 2007. Control of the B cell-intrinsic tolerance programs by ubiquitin ligases Cbl and Cbl-b. *Immunity*. 26:567–578. https://doi.org/10.1016/j.immuni.2007.03.015

Kräutler, N.J., D. Suan, D. Butt, K. Bourne, J.R. Hermes, T.D. Chan, C. Sundling, W. Kaplan, P. Schofield, J. Jackson, et al. 2017. Differentiation of germinal center B cells into plasma cells is initiated by high-affinity antigen and completed by Tfh cells. *J. Exp. Med.* 214:1259–1267. https://doi.org/10.1084/jem.20161533

Kurosaki, T., H. Shinohara, and Y. Baba. 2010. B cell signaling and fate decision. *Annu. Rev. Immunol.* 28:21–55. https://doi.org/10.1146/annurev.immunol.021908.132541

Kwak, K., N. Quizon, H. Sohn, A. Saniee, J. Manzella-Lapeira, P. Holla, J. Brzostowski, J. Lu, H. Xie, C. Xu, et al. 2018. Intrinsic properties of human germinal center B cells set antigen affinity thresholds. *Sci. Immunol.* 3:3. https://doi.org/10.1126/sciimmunol.aau6598

Lankar, D., H. Vincent-Schneider, V. Briken, T. Yokozeki, G. Raposo, and C. Bonnerot. 2002. Dynamics of major histocompatibility complex class II compartments during B cell receptor-mediated cell activation. *J. Exp. Med.* 195:461–472. https://doi.org/10.1084/jem.20011543

Lanzavecchia, A.. 1990. Receptor-mediated antigen uptake and its effect on antigen presentation to class II-restricted T lymphocytes. *Annu. Rev. Immunol.* 8:773–793. https://doi.org/10.1146/annurev.iy.08.040190.004013

Li, X., A. Gadzinsky, L. Gong, H. Tong, V. Calderon, Y. Li, D. Kitamura, U. Klein, W.Y. Langdon, F. Hou, et al. 2018. Cbl Ubiquitin Ligases Control B Cell Exit from the Germinal-Center Reaction. *Immunity*. 48:530–541.e6. https://doi.org/10.1016/j.immuni.2018.03.006

Liu, Y.J., D.E. Joshua, G.T. Williams, C.A. Smith, J. Gordon, and I.C. MacLennan. 1989. Mechanism of antigen-driven selection in germinal centres. *Nature*. 342:929–931. https://doi.org/10.1038/342929a0

Meli, A.P., G. Fontés, D.T. Avery, S.A. Leddon, M. Tam, M. Elliot, A. Ballesteros-Tato, J. Miller, M.M. Stevenson, D.J. Fowell, et al. 2016. The Integrin LFA-1 Controls T Follicular Helper Cell Generation and Maintenance. *Immunity*. 45:831–846. https://doi.org/10.1016/j.immuni.2016.09.018

Meyer-Hermann, M., E. Mohr, N. Pelletier, Y. Zhang, G.D. Victora, and K.M. Toellner. 2012. A theory of germinal center B cell selection, division, and exit. *Cell Rep.* 2:162–174. https://doi.org/10.1016/j.celrep.2012.05.010

Nowosad, C.R., K.M. Spillane, and P. Tolar. 2016. Germinal center B cells recognize antigen through a specialized immune synapse architecture. *Nat. Immunol.* 17:870–877. https://doi.org/10.1038/ni.3458

Oksvold, M.P., S.A. Dagger, C.B. Thien, and W.Y. Langdon. 2008. The Cbl-b RING finger domain has a limited role in regulating inflammatory cytokine production by IgE-activated mast cells. *Mol. Immunol.* 45: 925–936. https://doi.org/10.1016/j.molimm.2007.08.002

Phan, T.G., I. Grigorova, T. Okada, and J.G. Cyster. 2007. Subcapsular encounter and complement-dependent transport of immune complexes by lymph node B cells. *Nat. Immunol.* 8:992–1000. https://doi.org/10.1038/ni1494

Piper, R.C., I. Dikic, and G.L. Lukacs. 2014. Ubiquitin-dependent sorting in endocytosis. *Cold Spring Harb. Perspect. Biol.* 6. a016808. https://doi.org/10.1101/cshperspect.a016808

Qi, H., J.L. Cannons, F. Klauschen, P.L. Schwartzberg, and R.N. Germain. 2008. SAP-controlled T-B cell interactions underlie germinal centre formation. *Nature.* 455:764–769. https://doi.org/10.1038/nature07345

Rajewsky, K.. 1996. Clonal selection and learning in the antibody system. *Nature.* 381:751–758. https://doi.org/10.1038/381751a0

Reth, M.. 1992. Antigen receptors on B lymphocytes. *Annu. Rev. Immunol.* 10: 97–121. https://doi.org/10.1146/annurev.iy.10.040192.000525

Schwickert, T.A., R.L. Lindquist, G. Shakhar, G. Livshits, D. Skokos, M.H. Kosco-Vilbois, M.L. Dustin, and M.C. Nussenzweig. 2007. In vivo imaging of germinal centres reveals a dynamic open structure. *Nature.* 446:83–87. https://doi.org/10.1038/nature05573

Shlomchik, M.J., and F. Weisel. 2012a. Germinal center selection and the development of memory B and plasma cells. *Immunol. Rev.* 247:52–63. https://doi.org/10.1111/j.1600-065X.2012.01124.x

Shlomchik, M.J., and F. Weisel. 2012b. Germinal centers. *Immunol. Rev.* 247: 5–10. https://doi.org/10.1111/j.1600-065X.2012.01125.x

Shulman, Z., A.D. Gitlin, J.S. Weinstein, B. Lainez, E. Esplugues, R.A. Flavell, J.E. Craft, and M.C. Nussenzweig. 2014. Dynamic signaling by T follicular helper cells during germinal center B cell selection. *Science.* 345:1058–1062. https://doi.org/10.1126/science.1257861

Stoddart, A., M.L. Dykstra, B.K. Brown, W. Song, S.K. Pierce, and F.M. Brodsky. 2002. Lipid rafts unite signaling cascades with clathrin to regulate BCR internalization. *Immunity.* 17:451–462. https://doi.org/10.1016/S1074-7613(02)00416-8

Veselits, M., A. Tanaka, Y. Chen, K. Hamel, M. Mandal, M. Kandasamy, B. Manicassamy, S.K. O'Neill, P. Wilson, R. Sciammas, et al. 2017. Igβ ubiquitination activates PI3K signals required for endosomal sorting. *J. Exp. Med.* 214:3775–3790. https://doi.org/10.1084/jem.20161868

Victora, G.D., and M.C. Nussenzweig. 2012. Germinal centers. *Annu. Rev. Immunol.* 30:429–457. https://doi.org/10.1146/annurev-immunol-020711-075032

Watanabe, M., C. Fujihara, A.J. Radtke, Y.J. Chiang, S. Bhatia, R.N. Germain, and R.J. Hodes. 2017. Co-stimulatory function in primary germinal center responses: CD40 and B7 are required on distinct antigen-presenting cells. *J. Exp. Med.* 214:2795–2810. https://doi.org/10.1084/jem.20161955

Weinstein, J.S., E.I. Herman, B. Lainez, P. Licona-Limón, E. Esplugues, R. Flavell, and J. Craft. 2016. TFH cells progressively differentiate to regulate the germinal center response. *Nat. Immunol.* 17:1197–1205. https://doi.org/10.1038/ni.3554

Yuseff, M.I., P. Pierobon, A. Reversat, and A.M. Lennon-Duménil. 2013. How B cells capture, process and present antigens: a crucial role for cell polarity. *Nat. Rev. Immunol.* 13:475–486. https://doi.org/10.1038/nri3469

Zhang, M., M. Veselits, S. O'Neill, P. Hou, A.L. Reddi, I. Berlin, M. Ikeda, P.D. Nash, R. Longnecker, H. Band, et al. 2007. Ubiquitinylation of Ig beta dictates the endocytic fate of the B cell antigen receptor. *J. Immunol.* 179: 4435–4443. https://doi.org/10.4049/jimmunol.179.7.4435

Zotos, D., and D.M. Tarlinton. 2012. Determining germinal centre B cell fate. *Trends Immunol.* 33:281–288. https://doi.org/10.1016/j.it.2012.04.003

Supplemental material

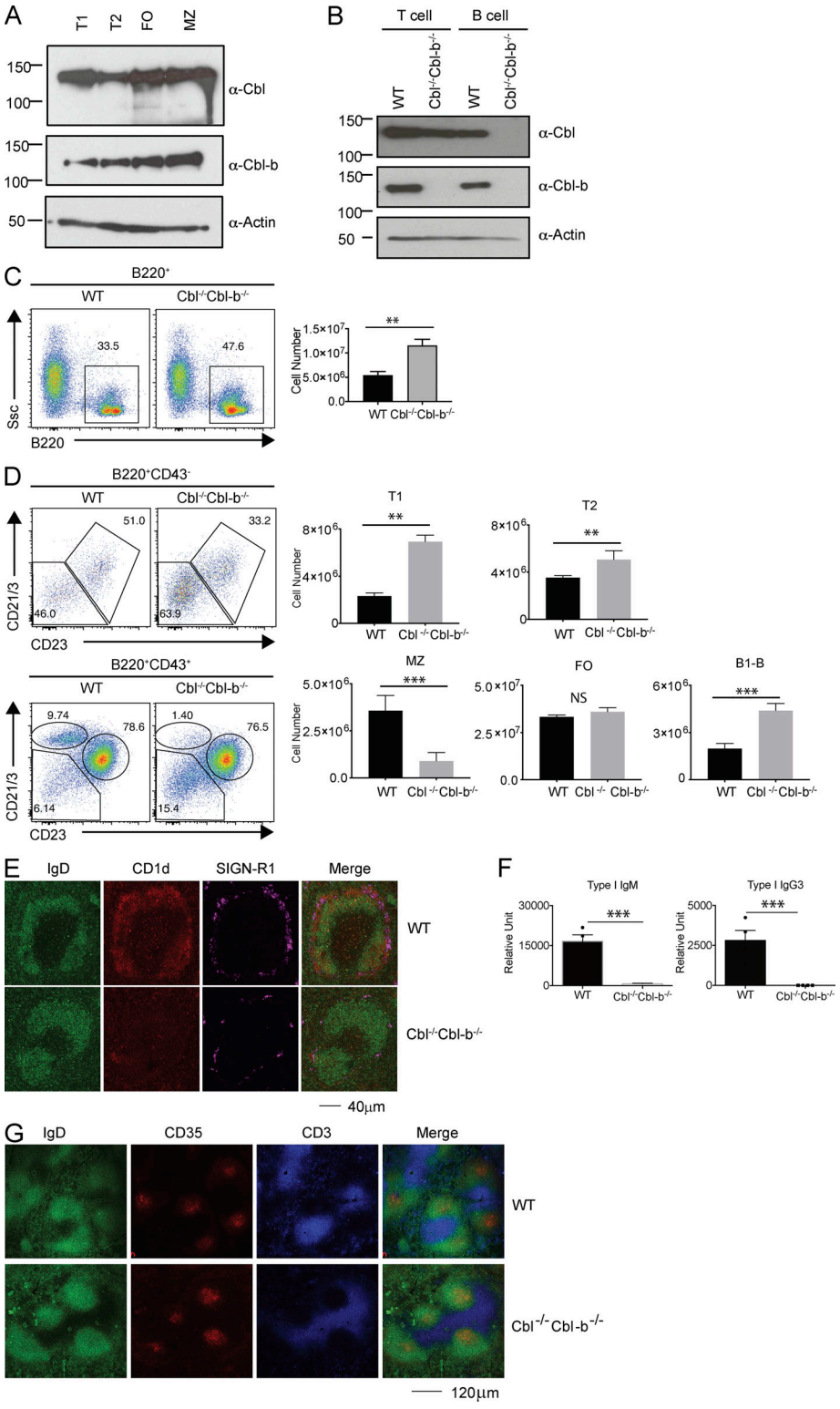

Figure S1. **General development of Cbl$^{-/-}$Cbl-b$^{-/-}$ B cells. (A)** Western blot analysis of Cbls expression in different subsets of splenic B cells (n = 2). FO, follicular. **(B)** Western blot analysis of Cbls deletion in B cells from Cbl$^{-/-}$Cbl-b$^{-/-}$ mice (n = 2). **(C)** Bone marrow B cells in Cbl$^{-/-}$Cbl-b$^{-/-}$ mice. Shown are flow cytometric analysis of B220^{+} B cells in the bone marrow. Absolute numbers of B cells are shown as bar representations (n = 5). **(D)** B cell development in Cbl$^{-/-}$Cbl-b$^{-/-}$ mice. Shown are flow cytometric analysis of splenic B cells stained with anti-CD21 and CD23. Immature transitional T1 and T2 cells and mature B1-b, follicular, and MZ B cells are schematically indicated (right). Absolute numbers of B cell in each subset are shown as bar representations (n = 5). **(E)** Immunofluorescent staining of spleen follicles. Shown are immunofluorescence image of B cell follicles stained with anti-IgD (green), anti-CD1d (red), or anti-Sign-R1 (pink). **(G)** ELISA analysis of serum type-I T cell–independent anti-NP responses (n = 4). **(H)** Immunofluorescent staining of spleen follicles from unimmunized mice. Shown are immunofluorescence image of B cell follicles stained with anti-IgD (green), anti-CD35 (red), and anti-CD3 (blue). Data are mean ± SEM of at least two independent experiments (C, D, and F). **, P < 0.01; ***, P < 0.001.

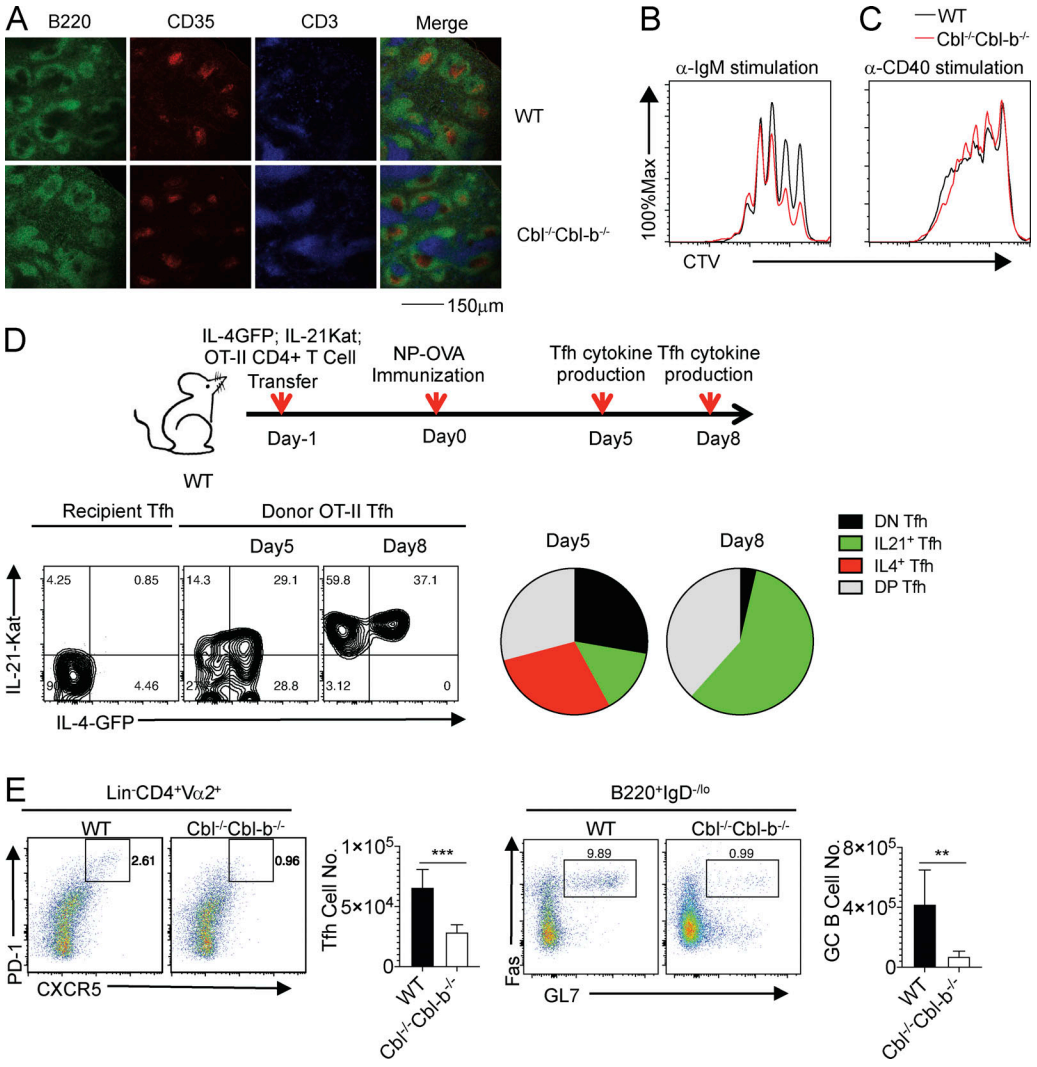

Figure S2. **Analyses of GC and Tfh cell development. (A)** Immunofluorescent staining of FDCs in WT and Cbl$^{-/-}$Cbl-b$^{-/-}$ mice. Shown are spleen sections of B cell follicles and FDCs stained with anti-B220 (green), anti-CD35 (red), and anti-CD3. **(B and C)** B cell proliferation assay. Shown are flow cytometric analyses of B cell proliferation after anti-IgM (B) or anti-CD40 (C) stimulation for three days. **(D)** System to examine Tfh cell development. Top: Scheme to examine Tfh cell development using IL4^{GFP}IL21^{Kat} OT-II T cell chimeric mice. Bottom: flow cytometric analyses of IL21^{Kat} vs. IL4^{GFP} expression in Tfh cells (left). Pie representations show the percentages of IL21^{+}, IL4^{+} or IL21^{+}IL4^{+} Tfh cells (n = 3). **(E)** Tfh and GC B cell development in WT and Cbl$^{-/-}$Cbl-b$^{-/-}$ recipient mice transplanted with IL4^{GFP}IL21^{Kat} OT-II T cells after NP-KLH immunization. Shown are FACS contour maps of PD-1 vs. CXCR5 staining of Tfh cells (left) and Fas vs. GL7 staining of GC B cells (right). IL4^{GFP}IL21^{Kat} expression in gated Tfh cells is shown in Fig. 2 C (n = 6). Data are mean ± SEM of at least two independent experiments (E). **, P < 0.01; ***, P < 0.001.

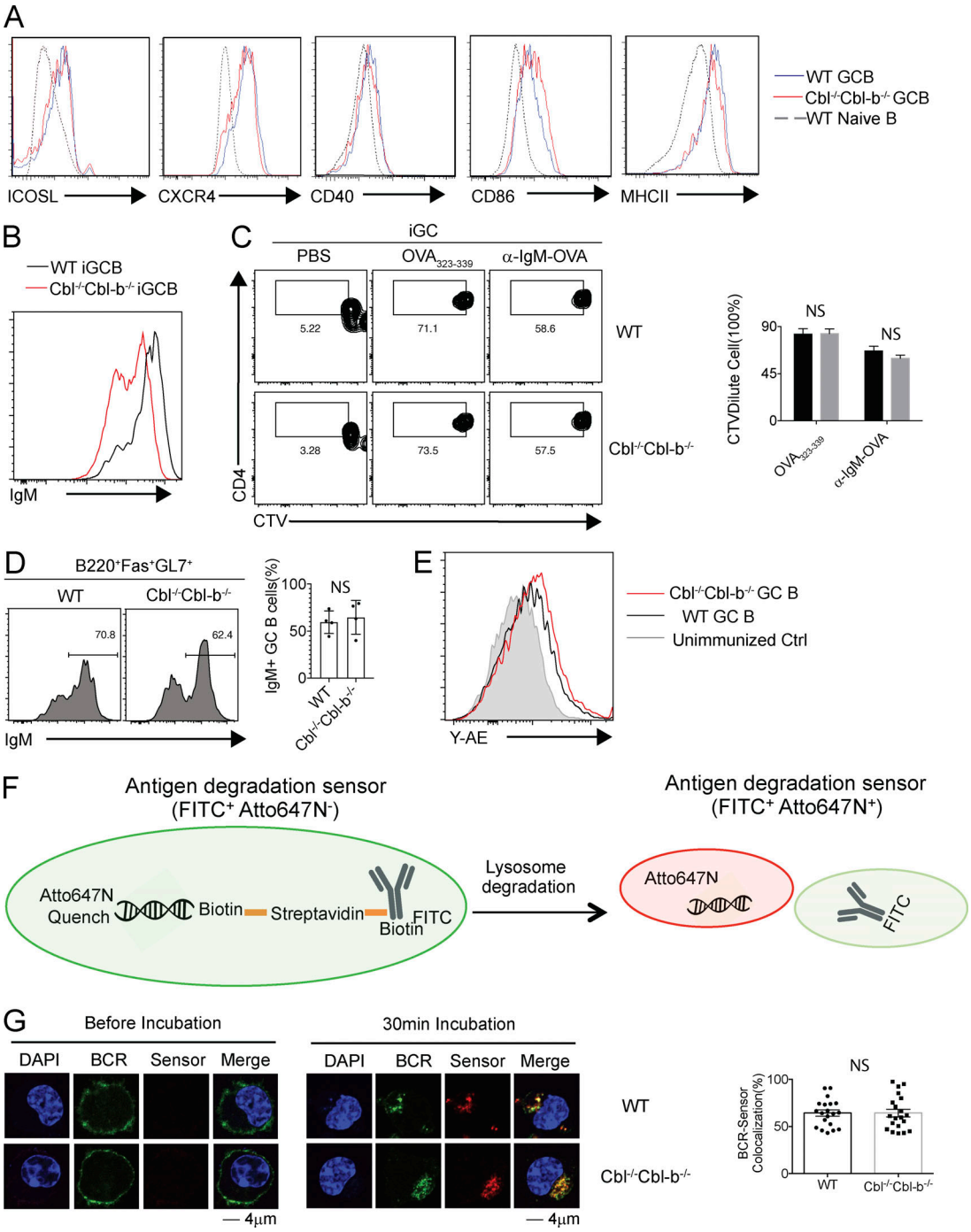

Figure S3. **BCR downmodulation and intracellular trafficking. (A)** Expression of costimulatory ligands and receptors on WT and Cbl$^{-/-}$Cbl-b$^{-/-}$ B cells. Shown are histogram analyses of IcosL, Cxcr4, CD40, CD86, and MHC-II expression on WT and Cbl$^{-/-}$Cbl-b$^{-/-}$ GC B cells. **(B)** Cell surface IgM expression on 40LB culture–derived WT and Cbl$^{-/-}$Cbl-b$^{-/-}$ iGC B cells. **(C)** OT-II T cell proliferation stimulated by OVA$_{323–339}$ peptide or anti-IgM-OVA antigen–loaded iGC B cells. Proliferation of OT-II T cells was measured based on the dilution of CTV fluorescent intensity. Shown are contour maps (left) of CTV intensity and statistics (right) of the gated OT-II T cells (n = 4). **(D)** Expression of cell surface IgM on WT and Cbl$^{-/-}$Cbl-b$^{-/-}$ GC B cells. Shown are histograms (left) and statistics (right) of cell surface IgM expression on gated GC B cells (n = 5). **(E)** In vivo presentation of antigen Eα-GFP by WT and Cbl$^{-/-}$Cbl-b$^{-/-}$ GC B cells. Shown is a histogram of Eα pMHC-II Y-Ae expression on gated WT and Cbl$^{-/-}$Cbl-b$^{-/-}$ GC cells (n = 3). **(F)** Scheme for generation and working principle of the lysosome degradation sensor. **(G)** BCR-mediated lysosome sensor degradation in WT and Cbl$^{-/-}$Cbl-b$^{-/-}$ iGC B cells. Shown are confocal images (left) and statistics (right) of GC B cells staining with anti-BCR lysosome degradation sensor before (top panel) and after (bottom panel) 30-min incubation at 37°C. Data represent mean ± SEM of at least two independent experiments (C, D, and G).

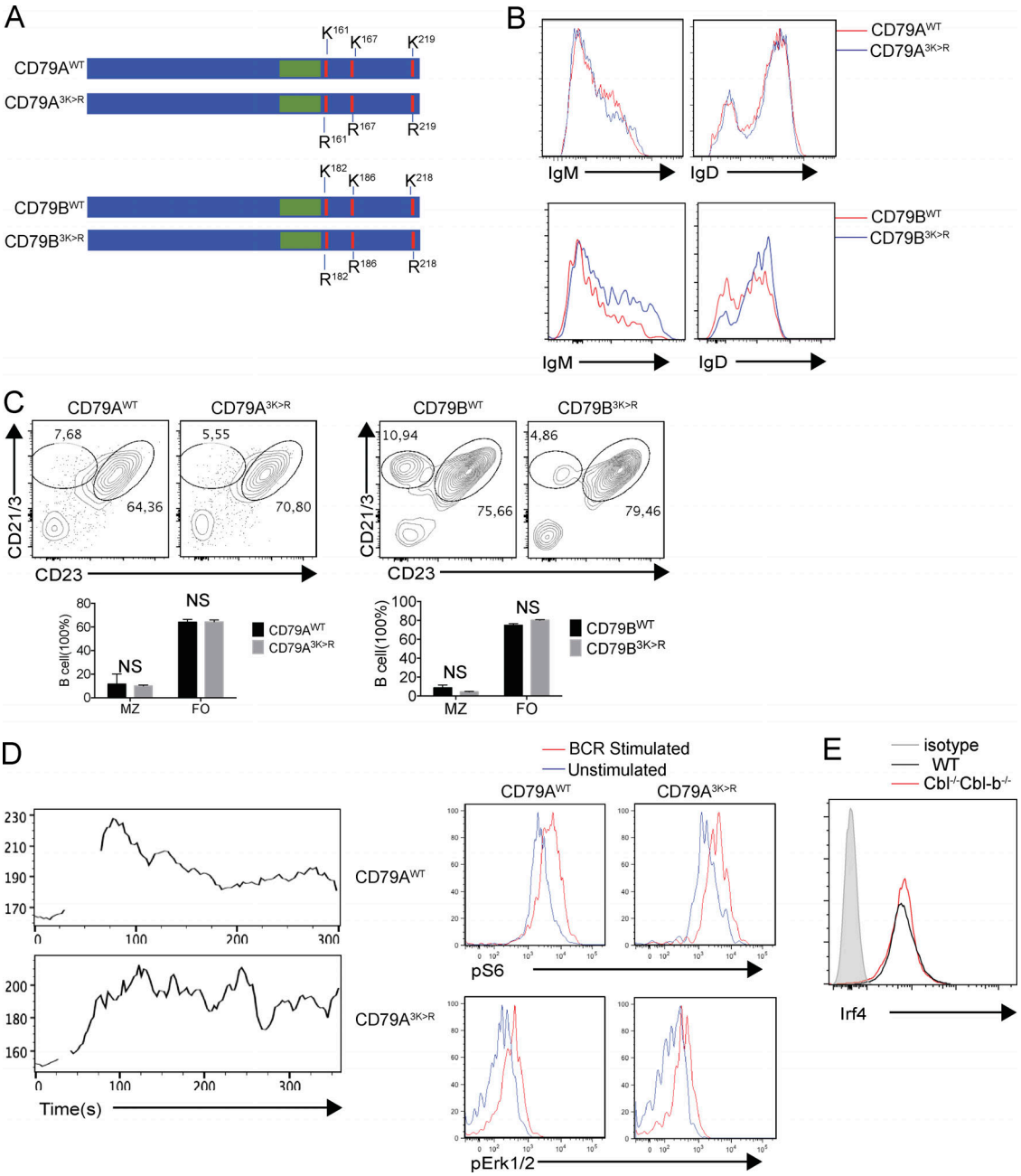

Figure S4. **CD79A and CD79B mutagenesis studies. (A)** Schematic of CD79A and CD79B mutations to block ubiquitination. **(B)** Histogram analyses of IgM and IgD staining of WT vs. CD79A$^{3K>R}$ or WT vs. CD79B$^{3K>R}$ splenic B cells from the corresponding BM chimeric mice (n = 3). **(C)** FACS analyses of CD21 vs. CD23 staining of B cell development in WT, CD79A$^{3K>R}$, and CD79B$^{3K>R}$ BM chimeric mice (n = 3). **(D)** FACS analysis of BCR-induced signaling in WT and CD79A$^{3K>R}$ B cells. Shown are histograms of Ca^{2+} influx (left), pS6 (top right), and pErk1/2 (bottom right) in unstimulated and BCR-stimulated B cells (n = 3). **(E)** FACS analyses of IRF4 expression in WT and Cbl$^{-/-}$Cbl-b$^{-/-}$ naive B cells (n = 3). Data are shown as mean ± SEM of two independent experiments (C–E).

Provided online are two tables. Table S1 lists the primers and gRNAs used in this study. Table S2 lists the antibodies used for flow cytometry.